BRL

CONTRACT REPORT BRL-CR-536

ARO-17888.2-EG

PROJECTILE MOTION IN A FLEXIBLE GUN TUBE

Prepared by

S&D Dynamics, Inc.
755 New York Ave.
Huntington, NY 11743

October 1984

US ARMY BALLISTIC RESEARCH LABORATORY
ABERDEEN PROVING GROUND, MARYLAND

Destroy this report when it is no longer needed.
Do not return it to the originator.

Additional copies of this report may be obtained from the National Technical Information Service, U. S. Department of Commerce, Springfield, Virginia 22161.

The findings in this report are not to be construed as an official Department of the Army position, unless so designated by other authorized documents.

The use of trade names or manufacturers' names in this report does not constitute indorsement of any commercial product.

UNCLASSIFIED

SECURITY CLASSIFICATION OF THIS PAGE (When Data Entered)

REPORT DOCUMENTATION PAGE

READ INSTRUCTIONS BEFORE COMPLETING FORM

1. REPORT NUMBER: Contract Report BRL-CR-536	2. GOVT ACCESSION NO.: AD-A149027
3. RECIPIENT'S CATALOG NUMBER	
4. TITLE (and Subtitle): PROJECTILE MOTION IN A FLEXIBLE GUN TUBE	5. TYPE OF REPORT & PERIOD COVERED: Final Report, 15 Nov 82 - 15 Mar 84
	6. PERFORMING ORG. REPORT NUMBER
7. AUTHOR(s): Martin T. Soifer, Robert S. Becker	8. CONTRACT OR GRANT NUMBER(s): DAAG29-83-C-0004
9. PERFORMING ORGANIZATION NAME AND ADDRESS: S&D Dynamics, Inc., 755 New York Ave., Huntington, N.Y. 11743	10. PROGRAM ELEMENT, PROJECT, TASK AREA & WORK UNIT NUMBERS: 1L162618AH80
11. CONTROLLING OFFICE NAME AND ADDRESS: US Army Ballistic Research Laboratory, ATTN: AMXBR-OD-ST, Aberdeen Proving Ground, MD 21005-5066	12. REPORT DATE: October 1984
	13. NUMBER OF PAGES: 88
14. MONITORING AGENCY NAME & ADDRESS (if different from Controlling Office)	15. SECURITY CLASS. (of this report): Unclassified
	15a. DECLASSIFICATION/DOWNGRADING SCHEDULE

16. DISTRIBUTION STATEMENT (of this Report)

Approved for public release; distribution unlimited.

17. DISTRIBUTION STATEMENT (of the abstract entered in Block 20, if different from Report)

18. SUPPLEMENTARY NOTES

19. KEY WORDS (Continue on reverse side if necessary and identify by block number)

Projectile Dynamics
Projectile In-Bore Motion
Projectile In-Bore Loading
Projectile/Gun-Tube Interaction
Gun Dynamics
Gun Tube Motion

20. ABSTRACT (Continue on reverse side if necessary and identify by block number)

A general, six degree-of-freedom model of a projectile of finite geometry and inertia traveling in a flexible, rifled or smoothbore gun tube has been developed. The model accommodates projectile spin, mass eccentricity, projectile/bore interfacial friction, elastic/plastic deformation of the projectile rotating band, and balloting--including bourrelet impact and rebound with the bore. The model is unrestricted regarding gun tube motion, and provides the ability to assess the

(continued on next page)

DD FORM 1 JAN 73 1473 EDITION OF 1 NOV 65 IS OBSOLETE

UNCLASSIFIED

SECURITY CLASSIFICATION OF THIS PAGE (When Data Entered)

20. (continued)

mutual effects of projectile/gun-tube interaction when solved simultaneously with the equations of a compatible gun dynamics simulation, such as DYNACODE-G. The basic formulation has been compared with other projectile in-bore motion formulations and descriptions appearing in recent literature, and is considered to be the most general developed to date. In addition, the model has been correlated with experimental in-bore radar doppler data obtained from firings of a specially designed 37mm weapon, and has demonstrated excellent theoretical/experimental agreement.

TABLE OF CONTENTS

LIST OF ILLUSTRATIONS

SECTION 1

INTRODUCTION

This final report has been prepared by S&D Dynamics, Inc. under contract DAAG29-83-C-0004 to the U.S. Army Research Office, Durham, N.C., with funding provided by the U.S. Army Ballistic Research Laboratory, Aberdeen Proving Ground, MD.

In accordance with the contract scope-of-work, this report documents our development of a general, six degree-of-freedom model of a projectile of finite geometry and inertia traveling in a flexible, rifled or smoothbore gun tube. The model accommodates projectile spin, mass eccentricity, projectile/bore interfacial friction, elastic/plastic deformation of the projectile rotating band, and balloting--including bourrelet impact and rebound with the bore. In addition, the model has been formulated in terms of gun tube motion parameters, thereby rendering the ability to assess the mutual effects of projectile/gun-tube interaction during in-bore motion when incorporated within, and solved simultaneously with, the equations of a compatible gun dynamics simulation, such as DYNACODE-G (Refs. 1,2). Furthermore, incorporation of this model within DYNACODE-G provides refinement of the latter, by replacement of the traveling point-mass projectile description presently contained therein with a physically realistic, interacting projectile description, as well as extension of the latter to rifled bore applications. Detailed development of the model is presented in Section 2.

The basic formulation comprising the model herein developed has been compared with other projectile in-bore motion formulations and descriptions appearing in recent literature. A summary of this comparison is presented in Section 3. As will be seen, the model herein developed appears to be the most general developed to date and, consequently, offers the broadest range of applicability.

In view of the potential applicability of the model herein developed, it was deemed prudent to attempt validation of the model on its own merits (prior to incorporation within DYNACODE-G), via correlation of model predictions with experimental in-bore projectile motion data for firings in an environment reasonably free of gun-tube motion. To achieve this objective, the U.S. Army Ballistic Research Laboratory, and, in particular, Mr. James O. Pilcher II and Dr. James N. Walbert of the Mechanics and Structures Branch of the Interior

Ballistics Division, provided in-bore radar doppler data for firings of two distinct projectile designs, from a specially designed 37mm weapon. Detailed documentation of the correlation effort performed, and the excellent theoretical/experimental agreement demonstrated, as well as pertinent general observations, are presented in Section 4.

The solution technique required to incorporate the model herein developed within DYNACODE-G, and thereby provide the desired refinement and extension of the latter, is discussed in detail in Section 5. In particular, considerations regarding the integration scheme and required step-size(s) for integration (since the frequency content in projectile motion is generally orders of magnitude greater than the frequency content in basic gun tube motion) are given special emphasis.

Finally, conclusions based on our findings and recommendations for further study are presented in Section 6.

SECTION 2

FORMULATION OF PROJECTILE EQUATIONS OF MOTION

In the interest of accommodating both rifled and smoothbore firings, the formulation herein presented is developed for a rifled bore gun tube, with relaxation of the rifling constraint introduced where necessary to accommodate a smoothbore gun tube. In addition, it is understood that the projectile rotating-band is to be interpreted as a bore-riding surface in the smoothbore application.

The system of simultaneous differential equations which describes the general, six degree-of-freedom motion of a projectile traveling in a flexible gun tube is formulated first in terms of the applied loads and moments acting on the projectile (Section 2.1). Based on practical limitations of projectile motion relative to the gun tube, consideration is given next to simplifying the general expressions obtained for the projectile angular velocity and acceleration (Section 2.2). Finally, the applied loads and moments acting on the projectile are defined via modeling of the projectile/gun-tube interaction and interior ballistics processes (Section 2.3), thereby completing the desired formulation.

It is noted that the formulation herein developed is, within the framework of the assumptions introduced, complete to within the prescription of gun tube motion. It is further noted that to fully account for the mutual effects of projectile/gun-tube interaction, such prescription may not be made independently but rather requires the simultaneous solution of this formulation with a compatible gun dynamics simulation, such as DYNACODE-G.

2.1 Projectile Equations of Motion in Terms of Applied Loads and Moments

The projectile is characterized as follows:

(i) the projectile consists of a main body, rotating band and bourrelet;

(ii) the projectile main-body behaves as a rigid body of finite geometry and inertia;

(iii) the rotating band behaves elastically, with allowance for deformation in the plastic regime;

(iv) the bourrelet behaves elastically, with allowance for impact and rebound with the bore;

(v) *eccentricity is permitted between the projectile c.g. and geometric center;*

(vi) *the projectile is permitted six degrees-of-freedom relative to the gun tube (whose motion is unrestricted), namely, three independent rotations of its main-body about its c.g. (corresponding to projectile pitch, yaw and roll relative to the gun tube) and three independent translations of its c.g.*

The following reference frames are introduced to facilitate tracking projectile motion:

(i) *S_o, with coordinates (x_o,y_o,z_o) and unit triad $(\hat{i}_o,\hat{j}_o,\hat{k}_o)$, is defined as an intermediate reference frame, fixed neither in the projectile nor in the gun tube, whose origin translates with the projectile along the gun tube axis and rotates with the projectile about the instantaneous tangent to the gun tube axis; $\hat{i}_o$ is directed toward the gun tube muzzle, along the instantaneous gun tube axis; at the initial projectile position, $\hat{j}_o$ is directed along the radius from the gun tube centerline to the projectile c.g.; $\hat{k}_o$ completes the triad;*

(ii) *S, with coordinates (x,y,z) and unit triad $(\hat{i},\hat{j},\hat{k})$, is defined as a body-fixed reference frame whose origin is fixed at the projectile c.g.; $\hat{i}$ is directed toward the projectile nose, parallel to its geometric axis; at the initial projectile position, $\hat{j}$ is parallel to $\hat{j}_o$; $\hat{k}$ completes the triad;*

(iii) *S', with coordinates (x',y',z') and unit triad $(\hat{i}',\hat{j}',\hat{k}')$, is defined as an inertial reference frame whose origin is fixed in space at the initial position of the origin of S_o and oriented (for convenience in subsequent applications of interest) parallel to the inertial reference frame defined in the gun dynamics simulation code, DYNACODE-G.*

The instantaneous orientations of S relative to S_o and S_o relative to S' are as depicted in Figures 1 and 2, respectively. Referring to these figures and the above definitions, it is noted that the kinematic relations between S_o and S' incorporate gun tube motions, as well as two of the six degrees-of-freedom of the projectile relative to the gun tube, namely, translational motion along the gun tube axis and spin (both of which may either be prescribed by interior ballistics

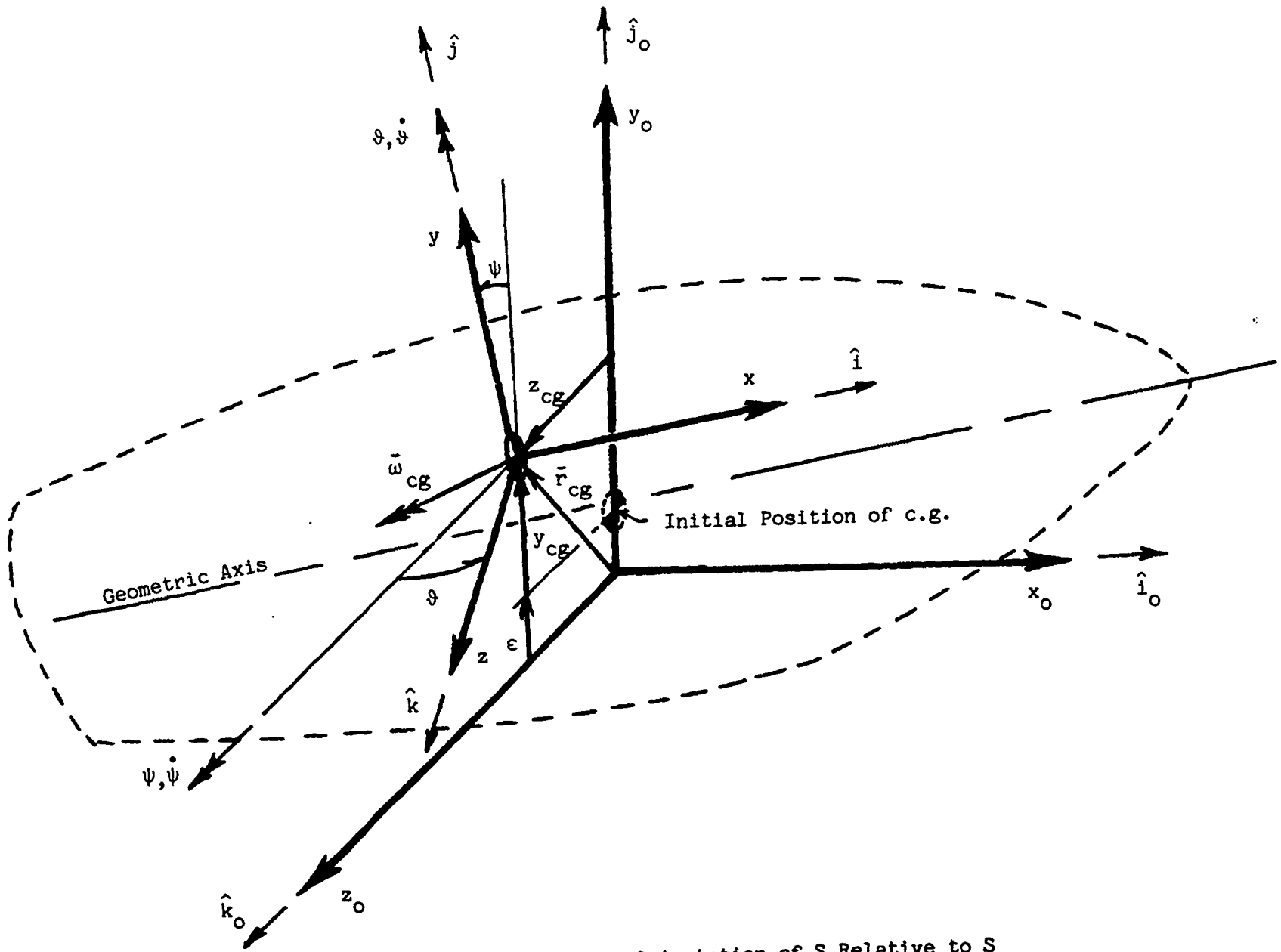

Figure 1 - Instantaneous Orientation of S Relative to S_o

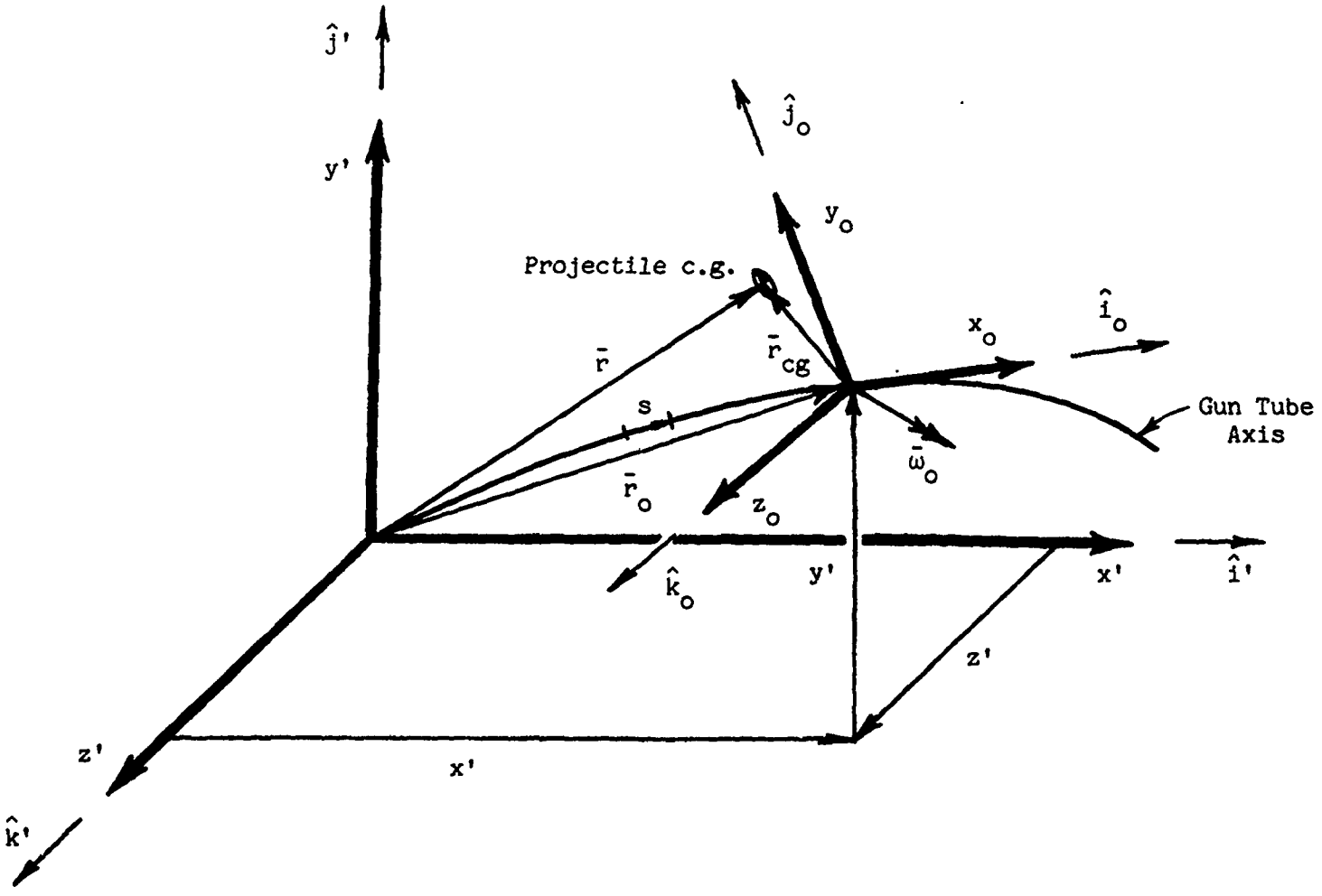

Figure 2 - Instantaneous Orientation of S_o Relative to S'

data or compatibly determined within the context of this formulation). Referring to Figure 1, the remaining four degrees-of-freedom of the projectile relative to the gun tube, namely, the two translational displacements y_{cg} and z_{cg} of the projectile c.g. in the $\hat{j}_o$-$\hat{k}_o$ plane and the two Euler angles ψ and ϑ, corresponding respectively to projectile pitch and yaw, are formulated in S relative to S_o.

Referring to Figure 2, the instantaneous position vector of the origin of S_o relative to S', namely $\bar{r}_o$, has components which are functions of time, t, as well as distance along the gun tube axis, s; that is

$$\bar{r}_o(s,t) = x'(s,t)\,\hat{i}' + y'(s,t)\,\hat{j}' + z'(s,t)\,\hat{k}' \quad . \tag{1}$$

Hence, noting that S' is fixed in space, and that

$$\frac{d(\ )}{dt} = \frac{\partial(\ )}{\partial t} + v_p \frac{\partial(\ )}{\partial s} \tag{2}$$

where v_p (= ds/dt) denotes the instantaneous velocity of S_o along the gun tube axis (i.e., the projectile velocity as prescribed by interior ballistics data), the instantaneous velocity of S_o relative to S', namely $\bar{v}_o$ (= $d\bar{r}_o/dt$), is given by

$$\bar{v}_o(s,t) = \left[\frac{\partial x'}{\partial t} + v_p \frac{\partial x'}{\partial s}\right] \hat{i}' + \left[\frac{\partial y'}{\partial t} + v_p \frac{\partial y'}{\partial s}\right] \hat{j}' + \left[\frac{\partial z'}{\partial t} + v_p \frac{\partial z'}{\partial s}\right] \hat{k}' \quad . \tag{3}$$

Similarly, the instantaneous acceleration of S_o relative to S', namely $\bar{a}_o$ (= $d\bar{v}_o/dt$), is given by

$$\begin{aligned} \bar{a}_o(s,t) = {} & \left[\frac{\partial^2 x'}{\partial t^2} + 2\, v_p \frac{\partial^2 x'}{\partial s \partial t} + v_p^2 \frac{\partial^2 x'}{\partial s^2} + a_p \frac{\partial x'}{\partial s}\right] \hat{i}' \\ & + \left[\frac{\partial^2 y'}{\partial t^2} + 2\, v_p \frac{\partial^2 y'}{\partial s \partial t} + v_p^2 \frac{\partial^2 y'}{\partial s^2} + a_p \frac{\partial y'}{\partial s}\right] \hat{j}' \\ & + \left[\frac{\partial^2 z'}{\partial t^2} + 2\, v_p \frac{\partial^2 z'}{\partial s \partial t} + v_p^2 \frac{\partial^2 z'}{\partial s^2} + a_p \frac{\partial z'}{\partial s}\right] \hat{k}' \end{aligned} \tag{4}$$

where a_p denotes dv_p/dt.

Referring to the Appendix, the instantaneous orientation of S_o relative to S' is defined in terms of the Euler angles $(\psi_o, \vartheta_o, \varphi_o)$ via the transformation

$$\left.\begin{aligned} \hat{i}' &= \ell^o_{11}\,\hat{i}_o + \ell^o_{12}\,\hat{j}_o + \ell^o_{13}\,\hat{k}_o \\ \hat{j}' &= \ell^o_{21}\,\hat{i}_o + \ell^o_{22}\,\hat{j}_o + \ell^o_{23}\,\hat{k}_o \\ \hat{k}' &= \ell^o_{31}\,\hat{i}_o + \ell^o_{32}\,\hat{j}_o + \ell^o_{33}\,\hat{k}_o \end{aligned}\right\} \tag{5}$$

where,

$$\left.\begin{aligned} \ell^o_{11} &= \cos\psi_o \cos\vartheta_o \\ \ell^o_{12} &= \cos\psi_o \sin\vartheta_o \sin\varphi_o - \sin\psi_o \cos\varphi_o \\ \ell^o_{13} &= \cos\psi_o \sin\vartheta_o \cos\varphi_o + \sin\psi_o \sin\varphi_o \\ \ell^o_{21} &= \sin\psi_o \cos\vartheta_o \\ \ell^o_{22} &= \sin\psi_o \sin\vartheta_o \sin\varphi_o + \cos\psi_o \cos\varphi_o \\ \ell^o_{23} &= \sin\psi_o \sin\vartheta_o \cos\varphi_o - \cos\psi_o \sin\varphi_o \\ \ell^o_{31} &= -\sin\vartheta_o \\ \ell^o_{32} &= \cos\vartheta_o \sin\varphi_o \\ \ell^o_{33} &= \cos\vartheta_o \cos\varphi_o \end{aligned}\right\}. \tag{6}$$

Noting that $\hat{i}_o$ lies along the instantaneous tangent to the gun tube axis, it follows that

$$\frac{\partial x'}{\partial s} = \ell^o_{11} \;;\; \frac{\partial y'}{\partial s} = \ell^o_{21} \;;\; \frac{\partial z'}{\partial s} = \ell^o_{31}\,. \tag{7}$$

Hence, substituting equations (5) and (7) into equations (3) and (4) there results the expressions for the instantaneous translational velocity and acceleration of S_o relative to S' in the form

$$\bar{v}_o = v_{x_o}\,\hat{i}_o + v_{y_o}\,\hat{j}_o + v_{z_o}\,\hat{k}_o \tag{8}$$

where,

$$\left.\begin{aligned} v_{x_o} &= v_p + \ell^o_{11}\frac{\partial x'}{\partial t} + \ell^o_{21}\frac{\partial y'}{\partial t} + \ell^o_{31}\frac{\partial z'}{\partial t} \\ v_{y_o} &= \ell^o_{12}\frac{\partial x'}{\partial t} + \ell^o_{22}\frac{\partial y'}{\partial t} + \ell^o_{32}\frac{\partial z'}{\partial t} \\ v_{z_o} &= \ell^o_{13}\frac{\partial x'}{\partial t} + \ell^o_{23}\frac{\partial y'}{\partial t} + \ell^o_{33}\frac{\partial z'}{\partial t} \end{aligned}\right\} \tag{9}$$

and

$$\bar{a}_o = a_{x_o}\,\hat{i}_o + a_{y_o}\,\hat{j}_o + a_{z_o}\,\hat{k}_o \tag{10}$$

where,

$$\left.\begin{aligned} a_{x_o} &= a_p + \ell^o_{11}\frac{\partial^2 x'}{\partial t^2} + \ell^o_{21}\frac{\partial^2 y'}{\partial t^2} + \ell^o_{31}\frac{\partial^2 z'}{\partial t^2} \\ a_{y_o} &= \ell^o_{12}\frac{\partial^2 x'}{\partial t^2} + \ell^o_{22}\frac{\partial^2 y'}{\partial t^2} + \ell^o_{32}\frac{\partial^2 z'}{\partial t^2} + 2\,v_p\left[\frac{\partial \psi_o}{\partial t}\cos\vartheta_o\cos\varphi_o - \frac{\partial \vartheta_o}{\partial t}\sin\varphi_o\right] + v_p^2\left[\frac{\partial \psi_o}{\partial s}\cos\vartheta_o\cos\varphi_o - \frac{\partial \vartheta_o}{\partial s}\sin\varphi_o\right] \\ a_{z_o} &= \ell^o_{13}\frac{\partial^2 x'}{\partial t^2} + \ell^o_{23}\frac{\partial^2 y'}{\partial t^2} + \ell^o_{33}\frac{\partial^2 z'}{\partial t^2} - 2\,v_p\left[\frac{\partial \psi_o}{\partial t}\cos\vartheta_o\sin\varphi_o + \frac{\partial \vartheta_o}{\partial t}\cos\varphi_o\right] - v_p^2\left[\frac{\partial \psi_o}{\partial s}\cos\vartheta_o\sin\varphi_o + \frac{\partial \vartheta_o}{\partial s}\cos\varphi_o\right] \end{aligned}\right\}. \tag{11}$$

Since S_o is constrained to move with the gun tube in the $\hat{j}_o$-$\hat{k}_o$ plane, it has angular velocity, $\bar{\omega}_o$, relative to S'. The expression for $\bar{\omega}_o$ (written relative to S_o), is given as

$$\bar{\omega}_o = \omega_{x_o}\,\hat{i}_o + \omega_{y_o}\,\hat{j}_o + \omega_{z_o}\,\hat{k}_o \tag{12}$$

where (referring to the Appendix),

$$\left.\begin{aligned} \omega_{x_o} &= \dot{\varphi}_o - \dot{\psi}_o \sin\vartheta_o \\ \omega_{y_o} &= \dot{\vartheta}_o \cos\varphi_o + \dot{\psi}_o \cos\vartheta_o \sin\varphi_o \\ \omega_{z_o} &= -\dot{\vartheta}_o \sin\varphi_o + \dot{\psi}_o \cos\vartheta_o \cos\varphi_o \end{aligned}\right\} \tag{13}$$

and $\dot{\psi}_o$, $\dot{\vartheta}_o$ and $\dot{\varphi}_o$ are obtained applying equation (2).

Noting that for a rifled bore gun tube φ_o is a function of s only, and applying equation (2), there results the rifling constraint

$$\dot{\varphi}_o = t_w\, v_p \tag{14}$$

where t_w (= $d\varphi_o/ds$) denotes the rifling twist; which is a known function prescribed by the design characteristics of the gun tube rifling. Hence, $\dot{\varphi}_o$ is a known function of v_p for a rifled bore gun tube.

Considering a smoothbore gun tube, it is noted that investigators generally assume that $\dot{\varphi}_o$ is identically zero throughout the in-bore motion. However, as will be seen, projectile mass eccentricity, initial projectile/bore angular misalignment, as well as bourrelet/bore impact each give rise to non-zero values of $\dot{\varphi}_o$. Hence, $\dot{\varphi}_o$ is herein retained as an unknown (independent of v_p) for smoothbore applications.

Noting that

$$\frac{d(\bar{\ })}{dt} = \dot{(\bar{\ })} + \bar{\omega} \times (\bar{\ }) \tag{15}$$

and applying equation (15) to equation (12), there results the angular acceleration of S_o relative to S', in the form

$$\dot{\bar{\omega}}_o = \dot{\omega}_{x_o}\,\hat{i}_o + \dot{\omega}_{y_o}\,\hat{j}_o + \dot{\omega}_{z_o}\,\hat{k}_o \tag{16}$$

where (from equation (13)),

$$\left.\begin{aligned}
\dot{\omega}_{x_o} &= \ddot{\varphi}_o - \ddot{\psi}_o \sin\vartheta_o - \dot{\psi}_o \dot{\vartheta}_o \cos\vartheta_o \\
\dot{\omega}_{y_o} &= \ddot{\vartheta}_o \cos\varphi_o + \ddot{\psi}_o \cos\vartheta_o \sin\varphi_o - \dot{\psi}_o \dot{\vartheta}_o \sin\vartheta_o \sin\varphi_o + \omega_{z_o} \dot{\varphi}_o \\
\dot{\omega}_{z_o} &= -\ddot{\vartheta}_o \sin\varphi_o + \ddot{\psi}_o \cos\vartheta_o \cos\varphi_o - \dot{\psi}_o \dot{\vartheta}_o \sin\vartheta_o \cos\varphi_o - \omega_{y_o} \dot{\varphi}_o
\end{aligned}\right\}. \tag{17}$$

Equations (8), (10), (12) and (16) prescribe the translational and angular velocities and accelerations of S_o relative to S'; with the rifling constraint, equation (14), introduced for a rifled bore gun tube. It remains to prescribe the motion of the projectile c.g. relative to S_o and, finally, its motion relative to S'.

Letting $\bar{v}_{cg}$ and $\bar{a}_{cg}$ respectively denote the translational velocity and acceleration of S relative to S_o, it follows from Figure 1 that

$$\left.\begin{aligned}
\bar{v}_{cg} &= \dot{y}_{cg} \hat{j}_o + \dot{z}_{cg} \hat{k}_o \\
\bar{a}_{cg} &= \ddot{y}_{cg} \hat{j}_o + \ddot{z}_{cg} \hat{k}_o
\end{aligned}\right\}. \tag{18}$$

Letting $\bar{\omega}_{cg}$ denote the angular velocity of S relative to S_o, and further specifying that

$$\bar{\omega}_{cg} = \omega_{x_{cg}} \hat{i} + \omega_{y_{cg}} \hat{j} + \omega_{z_{cg}} \hat{k} \tag{19}$$

the components of $\bar{\omega}_{cg}$ are prescribed (analogous to equation (13)) as functions of the Euler angles (ψ,ϑ,φ) of S relative to S_o in the form

$$\left.\begin{aligned}
\omega_{x_{cg}} &= \dot{\varphi} - \dot{\psi} \sin\vartheta \\
\omega_{y_{cg}} &= \dot{\vartheta} \cos\varphi + \dot{\psi} \cos\vartheta \sin\varphi \\
\omega_{z_{cg}} &= -\dot{\vartheta} \sin\varphi + \dot{\psi} \cos\vartheta \cos\varphi
\end{aligned}\right\}. \tag{20}$$

Noting that S_o is prescribed to rotate with S, equation (19) must be subjected to the constraint

$$\bar{\omega}_{cg} \cdot \hat{i}_o = 0 \quad . \tag{21}$$

Introducing the transformation from S to S_o, namely

$$\left.\begin{aligned} \hat{i}_o &= \ell_{11}\,\hat{i} + \ell_{12}\,\hat{j} + \ell_{13}\,\hat{k} \\ \hat{j}_o &= \ell_{21}\,\hat{i} + \ell_{22}\,\hat{j} + \ell_{23}\,\hat{k} \\ \hat{k}_o &= \ell_{31}\,\hat{i} + \ell_{32}\,\hat{j} + \ell_{33}\,\hat{k} \end{aligned}\right\} \tag{22}$$

and noting that the direction cosines, ℓ_{ij}, are defined in terms of the Euler angles (ψ,ϑ,φ) analogous to the definition presented in equation (6), there results from equations (19) thru (22)

$$\dot{\varphi} = \left[\frac{\tan\psi}{\cos\vartheta}\right]\dot{\vartheta} \tag{23}$$

which prescribes the dependence between the Euler angles of S required to satisfy the constraint presented in equation (21).

Equations (18) and (19) (subject to equation (23)) respectively prescribe the translational and angular motions of the projectile c.g. relative to S_o. It remains to prescribe this motion relative to S'.

Referring again to Figure 2, the instantaneous position vector of S relative to S', namely $\bar{r}$, is given by

$$\bar{r} = \bar{r}_o + \bar{r}_{cg} \quad . \tag{24}$$

Hence, noting equation (15), the (absolute) translational velocity and acceleration of the projectile c.g. (relative to S'), namely $\bar{v}$ and $\bar{a}$, respectively, are given by

$$\left.\begin{aligned} \bar{v} &= \bar{v}_o + \bar{v}_{cg} + \bar{\omega}_o \times \bar{r}_{cg} \\ \bar{a} &= \bar{a}_o + \bar{a}_{cg} + 2\,\bar{\omega}_o \times \bar{v}_{cg} + \dot{\bar{\omega}}_o \times \bar{r}_{cg} + \bar{\omega}_o \times (\bar{\omega}_o \times \bar{r}_{cg}) \end{aligned}\right\} \quad . \tag{25}$$

Substituting equations (10), (12), (16), and (18) into equation (25) and, in particular, into the expression for $\bar{a}$ (which is required for application to the equations of motion of the projectile), there results

$$\bar{a} = [a_{x_o} + 2\omega_{y_o}\dot{z}_{cg} - 2\omega_{z_o}\dot{y}_{cg} + z_{cg}(\dot{\omega}_{y_o} + \omega_{x_o}\omega_{z_o}) - (y_{cg} + \varepsilon) \times (\dot{\omega}_{z_o} - \omega_{x_o}\omega_{y_o})]\hat{i}_o + [a_{y_o} + \ddot{y}_{cg} - 2\omega_{x_o}\dot{z}_{cg} - z_{cg}(\dot{\omega}_{x_o} - \omega_{z_o}\omega_{y_o}) - (y_{cg} + \varepsilon)(\omega_{x_o}^2 + \omega_{z_o}^2)]\hat{j}_o + [a_{z_o} + \ddot{z}_{cg} + 2\omega_{x_o}\dot{y}_{cg} + (y_{cg} + \varepsilon) \times (\dot{\omega}_{x_o} + \omega_{z_o}\omega_{y_o}) - z_{cg}(\omega_{x_o}^2 + \omega_{y_o}^2)]\hat{k}_o \quad . \tag{26}$$

The (total) angular velocity of the projectile (relative to S') is given by

$$\bar{\omega} = \bar{\omega}_o + \bar{\omega}_{cg} \quad . \tag{27}$$

Applying equation (15) to each vector on the right-hand side of equation (27) there results the (total) angular acceleration of the projectile (relative to S')

$$\dot{\bar{\omega}} = \dot{\bar{\omega}}_o + \dot{\bar{\omega}}_{cg} + \bar{\omega}_o \times \bar{\omega}_{cg} \quad . \tag{28}$$

Transforming equation (12) from S_o to S via equation (22) and substituting the result, along with equation (19), into equation (27), there results

$$\bar{\omega} = \omega_x \hat{i} + \omega_y \hat{j} + \omega_z \hat{k} \tag{29}$$

where,

$$\left.\begin{aligned} \omega_x &= \omega_{x_{cg}} + \ell_{11}\omega_{x_o} + \ell_{21}\omega_{y_o} + \ell_{31}\omega_{z_o} \\ \omega_y &= \omega_{y_{cg}} + \ell_{12}\omega_{x_o} + \ell_{22}\omega_{y_o} + \ell_{32}\omega_{z_o} \\ \omega_z &= \omega_{z_{cg}} + \ell_{13}\omega_{x_o} + \ell_{23}\omega_{y_o} + \ell_{33}\omega_{z_o} \end{aligned}\right\} \quad . \tag{30}$$

Transforming equation (16) from S_o to S via equation (22), differentiating the components of equation (19) with respect to time, and substituting these results, along with equation (19), into equation (28), there results

$$\dot{\bar{\omega}} = \dot{\omega}_x \hat{i} + \dot{\omega}_y \hat{j} + \dot{\omega}_z \hat{k} \tag{31}$$

where,

$$\left.\begin{aligned}
\dot{\omega}_x &= \dot{\omega}_{x_{cg}} + \ell_{11}\,\dot{\omega}_{x_o} + \ell_{21}\,\dot{\omega}_{y_o} + \ell_{31}\,\dot{\omega}_{z_o} + \omega_{y_{cg}}\,(\ell_{13}\,\omega_{x_o} + \ell_{23}\,\omega_{y_o} \\
&\quad + \ell_{33}\,\omega_{z_o}) - \omega_{z_{cg}}\,(\ell_{12}\,\omega_{x_o} + \ell_{22}\,\omega_{y_o} + \ell_{32}\,\omega_{z_o}) \\
\dot{\omega}_y &= \dot{\omega}_{y_{cg}} + \ell_{12}\,\dot{\omega}_{x_o} + \ell_{22}\,\dot{\omega}_{y_o} + \ell_{32}\,\dot{\omega}_{z_o} + \omega_{x_{cg}}\,(\ell_{13}\,\omega_{x_o} + \ell_{23}\,\omega_{y_o} \\
&\quad + \ell_{33}\,\omega_{z_o}) - \omega_{z_{cg}}\,(\ell_{11}\,\omega_{x_o} + \ell_{21}\,\omega_{y_o} + \ell_{31}\,\omega_{z_o}) \\
\dot{\omega}_z &= \dot{\omega}_{z_{cg}} + \ell_{13}\,\dot{\omega}_{x_o} + \ell_{23}\,\dot{\omega}_{y_o} + \ell_{33}\,\dot{\omega}_{z_o} - \omega_{x_{cg}}\,(\ell_{12}\,\omega_{x_o} + \ell_{22}\,\omega_{y_o} \\
&\quad + \ell_{32}\,\omega_{z_o}) + \omega_{y_{cg}}\,(\ell_{11}\,\omega_{x_o} + \ell_{21}\,\omega_{y_o} + \ell_{31}\,\omega_{z_o})
\end{aligned}\right\} \tag{32}$$

and (from equation (20)),

$$\left.\begin{aligned}
\dot{\omega}_{x_{cg}} &= \ddot{\varphi} - \ddot{\psi}\sin\vartheta - \dot{\psi}\,\dot{\vartheta}\cos\vartheta \\
\dot{\omega}_{y_{cg}} &= \ddot{\vartheta}\cos\varphi + \ddot{\psi}\cos\vartheta\sin\varphi - \dot{\psi}\,\dot{\vartheta}\sin\vartheta\sin\varphi + \omega_{z_{cg}}\,\dot{\varphi} \\
\dot{\omega}_{z_{cg}} &= -\ddot{\vartheta}\sin\varphi + \ddot{\psi}\cos\vartheta\cos\varphi - \dot{\psi}\,\dot{\vartheta}\sin\vartheta\cos\varphi - \omega_{y_{cg}}\,\dot{\varphi}
\end{aligned}\right\} \tag{33}$$

where (from equation (23)),

$$\ddot{\varphi} = \left[\frac{\tan\psi}{\cos\vartheta}\right]\ddot{\vartheta} + \frac{\dot{\vartheta}}{\cos\vartheta}\left[\frac{\dot{\psi}}{\cos^2\psi} + \dot{\vartheta}\tan\psi\tan\vartheta\right] . \tag{34}$$

We are now in a position to formulate the equations of motion of the projectile in terms of the applied loads and moments.

Letting $\bar{F}$ (which remains to be prescribed) denote the resultant applied force acting at the projectile c.g., and applying Newton's law of motion with $\bar{a}$ as prescribed in equation (26), there results the three scalar equations of translational motion of the projectile c.g. (written relative to S_o) in the form

$$\left.\begin{aligned}
F_{x_o} &= m_p \left[a_{x_o} - 2\,\omega_{z_o}\,\dot{y}_{cg} + 2\,\omega_{y_o}\,\dot{z}_{cg} - (y_{cg} + \varepsilon)\,(\dot{\omega}_{z_o} - \omega_{x_o}\,\omega_{y_o})\right. \\
&\qquad \left. + z_{cg}\,(\dot{\omega}_{y_o} + \omega_{x_o}\,\omega_{z_o})\right] \\
F_{y_o} &= m_p \left[a_{y_o} + \ddot{y}_{cg} - 2\,\omega_{x_o}\,\dot{z}_{cg} - (y_{cg} + \varepsilon)\,(\omega_{x_o}^2 + \omega_{z_o}^2)\right. \\
&\qquad \left. - z_{cg}\,(\dot{\omega}_{x_o} - \omega_{y_o}\,\omega_{z_o})\right] \\
F_{z_o} &= m_p \left[a_{z_o} + \ddot{z}_{cg} + 2\,\omega_{x_o}\,\dot{y}_{cg} + (y_{cg} + \varepsilon)\,(\dot{\omega}_{x_o} + \omega_{y_o}\,\omega_{z_o})\right. \\
&\qquad \left. - z_{cg}\,(\omega_{x_o}^2 + \omega_{y_o}^2)\right]
\end{aligned}\right\} \qquad (35)$$

where m_p denotes the mass of the projectile, and F_{x_o}, F_{y_o} and F_{z_o} denote the components of $\bar{F}$ along the respective axes of S_o.

Letting $\bar{M}$ (which also remains to be prescribed) denote the resultant applied moment acting about the projectile c.g., and applying the principle of angular momentum with $\bar{\omega}$ and $\dot{\bar{\omega}}$ prescribed respectively in equations (29) and (31), there results the three scalar equations of angular motion of the projectile about its c.g. (written relative to S in order to preclude introducing time derivatives of the projectile inertia tensor) in the form

$$\left.\begin{aligned}
M_x &= I_{xx}\,\dot{\omega}_x + (I_{zz} - I_{yy})\,\omega_y\,\omega_z + I_{xy}\,(\omega_x\,\omega_z - \dot{\omega}_y) - I_{xz}\,(\dot{\omega}_z \\
&\qquad + \omega_x\,\omega_y) - I_{yz}\,(\omega_y^2 - \omega_z^2)
\end{aligned}\right\} \approx$$

$$
\left.
\begin{aligned}
M_y &= I_{yy}\,\dot{\omega}_y + (I_{xx} - I_{zz})\,\omega_x\,\omega_z + I_{yz}\,(\omega_x\,\omega_y - \dot{\omega}_z) - I_{yx}\,(\dot{\omega}_x \\
&\quad + \omega_y\,\omega_z) + I_{zx}\,(\omega_x^2 - \omega_z^2) \\
M_z &= I_{zz}\,\dot{\omega}_z - (I_{xx} - I_{yy})\,\omega_x\,\omega_y + I_{zx}\,(\omega_y\,\omega_z - \dot{\omega}_x) - I_{zy}\,(\dot{\omega}_y \\
&\quad + \omega_x\,\omega_z) - I_{xy}\,(\omega_x^2 - \omega_y^2)
\end{aligned}
\right\} \qquad (36)
$$

where M_x, M_y and M_z denote the components of $\bar{M}$ about the respective axes of S, and I_{xx}, I_{yy}, ..., I_{zy} denote the elements of the projectile inertia tensor written relative to S.

2.2 Simplification of Angular Velocity and Acceleration Expressions

The expressions for the terms representing the angular velocity and acceleration components entering equation (36) may be greatly simplified by noting that for most practical applications ψ and ϑ are sufficiently small such that

$$
\left.
\begin{aligned}
&\sin\psi \approx \psi \;\; ; \;\; \cos\psi \approx 1 \\
&\sin\vartheta \approx \vartheta \;\; ; \;\; \cos\vartheta \approx 1
\end{aligned}
\right\} . \qquad (37)
$$

Under this condition it follows from equation (23) that

$$
\dot{\varphi} \approx \psi\,\dot{\vartheta} \; . \qquad (38)
$$

Applying the mean value theorem, it follows that the integral of $\dot{\varphi}$ will at most be of order $\psi\,\vartheta$. Hence, to first order

$$
\varphi \approx 0 \; . \qquad (39)
$$

Imposing the above conditions and retaining only linear (first order) terms in ψ and ϑ, the direction cosines for the transformation from S to S_o, as given in equation (22), simplify to

$$\left.\begin{aligned} \ell_{11} &= \ell_{22} = \ell_{33} = 1 \\ \ell_{12} &= -\ell_{21} = -\psi \\ \ell_{13} &= -\ell_{31} = \vartheta \\ \ell_{23} &= \ell_{32} = 0 \end{aligned}\right\} \tag{40}$$

Noting the above, equations (20) and (33) simplify respectively to

$$\left.\begin{aligned} \omega_{x_{cg}} &\approx \psi\,\dot{\vartheta} - \vartheta\,\dot{\psi} \\ \omega_{y_{cg}} &\approx \dot{\vartheta} \\ \omega_{z_{cg}} &\approx \dot{\psi} \end{aligned}\right\} \tag{41}$$

and

$$\left.\begin{aligned} \dot{\omega}_{x_{cg}} &\approx \psi\,\ddot{\vartheta} - \vartheta\,\ddot{\psi} \\ \dot{\omega}_{y_{cg}} &\approx \ddot{\vartheta} + \psi\,\dot{\psi}\,\dot{\vartheta} \\ \dot{\omega}_{z_{cg}} &\approx \ddot{\psi} - \vartheta\,\dot{\vartheta}\,\dot{\psi} - \psi\,\dot{\vartheta}^2 \end{aligned}\right\} \tag{42}$$

Substituting equations (40) thru (42) into equations (30) and (32), there results the greatly simplified expressions for the angular velocity and acceleration components entering equation (36) in the form

$$\left.\begin{aligned} \omega_x &= \omega_{x_o} + \psi\,(\omega_{y_o} + \dot{\vartheta}) - \vartheta\,(\omega_{z_o} + \dot{\psi}) \\ \omega_y &= \omega_{y_o} + \dot{\vartheta} - \psi\,\omega_{x_o} \\ \omega_z &= \omega_{z_o} + \dot{\psi} + \vartheta\,\omega_{x_o} \end{aligned}\right\} \tag{43}$$

and

$$
\left.
\begin{aligned}
\dot{\omega}_x &= \dot{\omega}_{x_o} + \psi\,(\ddot{\vartheta} + \dot{\omega}_{y_o}) - \vartheta\,(\ddot{\psi} + \dot{\omega}_{z_o}) + \dot{\vartheta}\,(\vartheta\,\omega_{x_o} + \omega_{z_o}) \\
&\quad + \dot{\psi}\,(\psi\,\omega_{x_o} - \omega_{y_o}) \\
\dot{\omega}_y &= \dot{\omega}_{y_o} + \ddot{\vartheta} + \psi\,(\dot{\vartheta}\,\dot{\psi} - \dot{\omega}_{x_o}) - \dot{\psi}\,(\omega_{x_o} + \psi\,\omega_{y_o}) \\
&\quad + \psi\,\dot{\vartheta}\,(\vartheta\,\omega_{x_o} + \omega_{z_o}) \\
\dot{\omega}_z &= \dot{\omega}_{z_o} + \ddot{\psi} - \psi\,\dot{\vartheta}^2 - \vartheta\,(\dot{\vartheta}\,\dot{\psi} - \dot{\omega}_{x_o}) + \dot{\vartheta}\,(\omega_{x_o} - \vartheta\,\omega_{z_o}) \\
&\quad - \vartheta\,\dot{\psi}\,(\psi\,\omega_{x_o} - \omega_{y_o})
\end{aligned}
\right\} \quad (44)
$$

2.3 Applied Loads and Moments

The equations of projectile motion developed in the preceding section require specification of the applied loads, $\bar{F}$ (written relative to S_o), and the applied moments, $\bar{M}$ (written relative to S), for completion of the formulation. These loads and moments arise as a consequence of the projectile weight, interfacial contact of the rotating band and bourrelet with the bore, propellant gas pressure acting at the base of the projectile, and compressed air ahead of the projectile.

2.3.1 Projectile Weight Loading

The load applied to the projectile c.g. due to its own weight is given by

$$\bar{F}_w = - m_p\, g\, \hat{j}' \quad (45)$$

where m_p and g denote respectively the projectile mass and gravitational acceleration.

Applying the transformation given in equation (5), equation (45) is written relative to S_o for application to equation (35) in the form

$$\tilde{F}_w = F^w_{x_o}\,\hat{i}_o + F^w_{y_o}\,\hat{j}_o + F^w_{z_o}\,\hat{k}_o \tag{46}$$

where,

$$\left.\begin{aligned} F^w_{x_o} &= -\,m_p\,g\,\sin\psi_o\,\cos\vartheta_o \\ F^w_{y_o} &= -\,m_p\,g\,(\sin\psi_o\,\sin\vartheta_o\,\sin\varphi_o + \cos\psi_o\,\cos\varphi_o) \\ F^w_{z_o} &= -\,m_p\,g\,(\sin\psi_o\,\sin\vartheta_o\,\cos\varphi_o - \cos\psi_o\,\sin\varphi_o) \end{aligned}\right\}. \tag{47}$$

2.3.2 Rotating-Band/Bore Interfacial Contact Loading

The loads and moments applied at the projectile c.g. due to interfacial contact of the rotating band with the bore are derived subject to the following assumptions:

(i) *since modeling the engraving process in a rifled bore gun tube is beyond the scope of this effort, the initial state of the projectile and, in particular, the rotating band is defined here as its fully engraved state; hence, for this purpose, the initial state of the rotating band is characterized as a radially compressed elastic band with elastic/plastic boundary at the bore surface;*

(ii) *projectile motion subsequent to engraving induces additional elastic, as well as plastic radial deformations of the rotating band;*

(iii) *elastic radial deformation of the rotating band is characterized by a Winkler foundation model; rendering a radially directed rotating-band/bore interfacial load distribution (with local magnitude determined by resultant local radial displacement) which varies circumferentially around the bore, as well as longitudinally along the length of the interface; the latter variation gives rise to the so called "foundation" moment;*

(iv) *each cross-section of the rotating band maintains full contact with the bore;*

(v) *Coulomb friction acts at the rotating-band/bore interface; rendering a load distribution with magnitude proportional to the radially directed distribution and directed opposite to the resultant motion at the interface;*

(vi) *rifling torque is transmitted without slippage via a uniformly distributed circumferential load acting along the length of the rotating band at the rotating-band/bore interface;*

(vii) *the projectile main-body is rigid compared to the rotating band;*

(viii) *the Euler angles ψ and ϑ satisfy equation (37).*

In view of Assumptions (vii) and (viii), the displacement relative to S_o, namely $\bar{\delta}$, of any point of the projectile in a plane perpendicular to its geometric axis is, at any instant during the motion, given by

$$\bar{\delta} = (y_{cg} - \xi\,\psi)\,\hat{j}_o + (z_{cg} + \xi\,\vartheta)\,\hat{k}_o \tag{48}$$

where ξ denotes the perpendicular distance from the projectile c.g. to the plane of interest. It is noted that $\xi > 0$ implies that the plane of interest is aft of the projectile c.g.; $\xi = 0$ implies that the plane of interest contains the projectile c.g.; while $\xi < 0$ implies that the plane of interest is forward of the projectile c.g.

The radial component of this displacement, namely δ_r, is given as

$$\delta_r = \bar{\delta} \cdot \hat{i}_r = (y_{cg} - \xi\,\psi)\cos\varphi + (z_{cg} + \xi\,\vartheta)\sin\varphi \tag{49}$$

where φ denotes the angle between the projection of the y_o-axis onto the plane of interest and the line from the gun tube centerline to the point under consideration.

The maximum radial displacement, δ_{max}, in the plane of interest is determined by setting

$$\frac{\partial \delta_r}{\partial \varphi} = 0 \quad . \tag{50}$$

Letting φ_{max} denote the orientation of maximum radial displacement, there results from equations (49) and (50)

$$\varphi_{max} = \tan^{-1}\left[\frac{z_{cg} + \xi\,\vartheta}{y_{cg} - \xi\,\psi}\right] \tag{51}$$

and hence,

$$\delta_{max} = \sqrt{(y_{cg} - \xi\,\psi)^2 + (z_{cg} + \xi\,\vartheta)^2} \quad . \tag{52}$$

In view of equations (51) and (52), there results from equation (49)

$$\delta_r = \delta_{max} \cos(\varphi - \varphi_{max}) \tag{53}$$

which prescribes the circumferential distribution of radial displacement in the plane of interest. It is noted that this distribution is symmetric with respect to the angle φ_{max}. It is further noted that both δ_{max} and φ_{max} vary from one plane to the next in accordance with the variation of ξ. Hence, applying equations (51) thru (53) to planes containing the rotating band, it is seen that the radial deformation within a band cross-section is non-uniformly distributed around its circumference, and that both the magnitude and orientation of this distribution vary from one cross-section to the next along the length of the band.

Superposing the initial radial compression, δ_o, in accordance with Assumption (i), and multiplying by the elastic "spring" stiffness per unit surface area of the rotating band, k, there results in accordance with Assumption (iii), the radial load per unit surface area, $\bar{R}(\varphi,\xi)$, acting on the rotating band at the rotating-band/bore interface at each instant during the motion, in the form

$$\bar{R}(\varphi,\xi) = -k\,(\delta_r + \delta_o)\,\hat{i}_r \quad . \tag{54}$$

In view of Assumption (iv), the radial load distribution at a typical cross-section of the rotating band, as specified by equation (54) for a constant value of ξ, is as depicted in Figure 3.

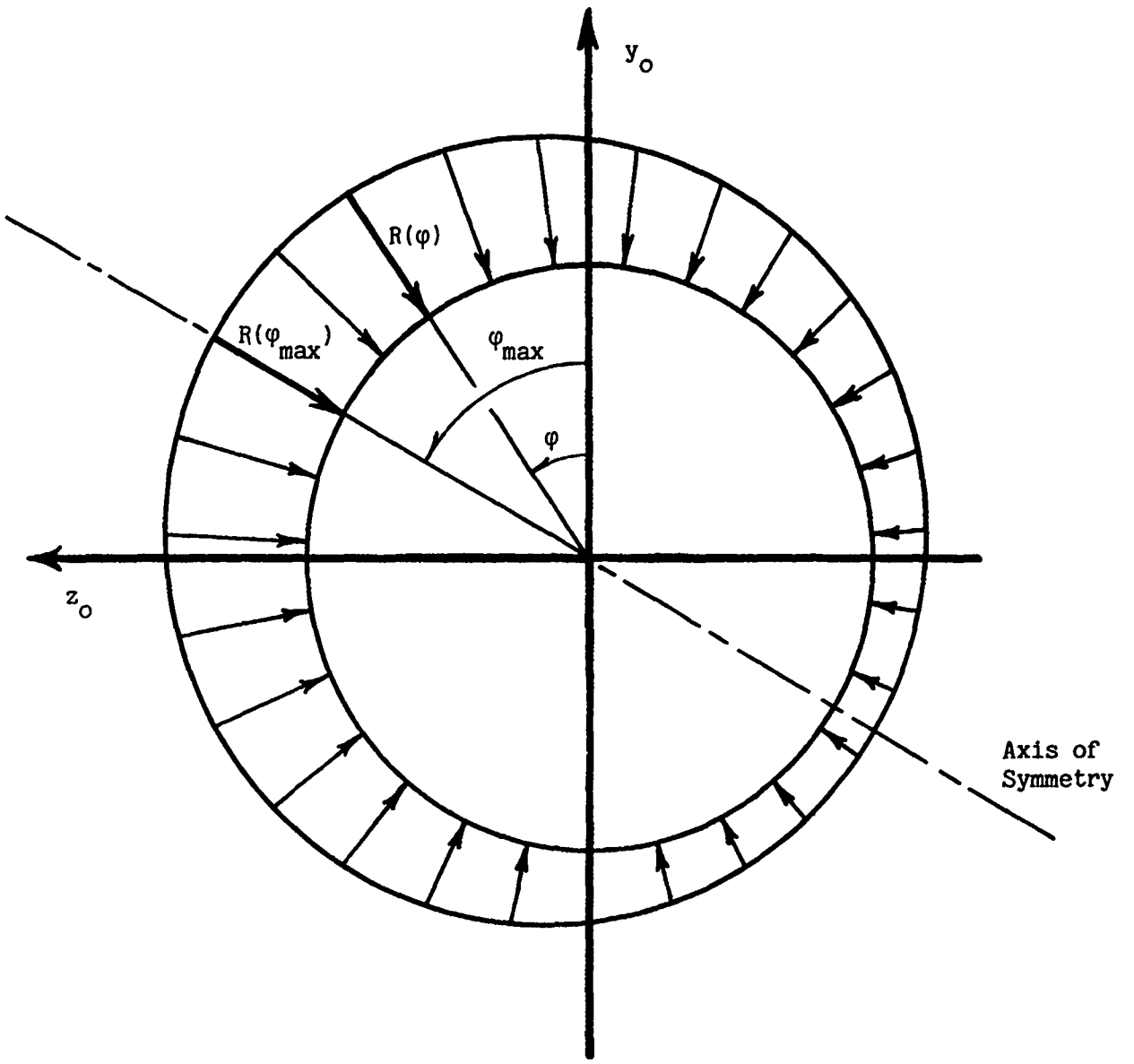

Figure 3 - Radial Load Distribution at Typical Cross-Section of Rotating Band

In view of Assumptions (iv) thru (vi), the instantaneous interfacial contact loads acting on a differential element of the rotating band are as depicted in Figure 4.

Under Assumption (v), the friction force, $\mu \bar{R}$, acts tangential to the bore surface in the direction opposing projectile motion at the surface. The angle α depicted in Figure 4 is determined from the expression

$$\tan \alpha = \begin{cases} r_b \, t_w & ; \quad \text{rifled bore} \\ \dfrac{r_b \, \dot{\varphi}_o}{v_p} & ; \quad \text{smoothbore} \end{cases} . \tag{55}$$

In addition, in accordance with Assumption (vi), the rifling-torque load per unit surface area of the rotating band, $\bar{T}$, is constant over the entire rotating-band/bore interface in a rifled bore gun tube; whereas, $\bar{T} \equiv 0$ for a smoothbore gun tube.

Letting $d\bar{F}_c$ denote the resultant incremental contact load acting on a differential element of the rotating band, it may be written in component form (relative to S_o) as

$$d\bar{F}_c = dF^c_{x_o} \, \hat{i}_o + dF^c_{y_o} \, \hat{j}_o + dF^c_{z_o} \, \hat{k}_o \tag{56}$$

where referring to Figure 4

$$\left.\begin{aligned} dF^c_{x_o} &= - r_b \, \mu \, R(\varphi,\xi) \cos \alpha \, d\xi \, d\varphi \\ dF^c_{y_o} &= r_b \, \{R(\varphi,\xi) \, [- \cos \varphi + \mu \sin \alpha \sin \varphi] - T \sin \varphi\} \, d\xi \, d\varphi \\ dF^c_{z_o} &= r_b \, \{R(\varphi,\xi) \, [- \sin \varphi - \mu \sin \alpha \cos \varphi] + T \cos \varphi\} \, d\xi \, d\varphi \end{aligned}\right\} . \tag{57}$$

Integrating over the rotating-band/bore interfacial surface area, there results, for application to equation (35), the contribution to the force components acting at the projectile c.g. (relative to S_o) due to rotating band contact with the bore, as follows

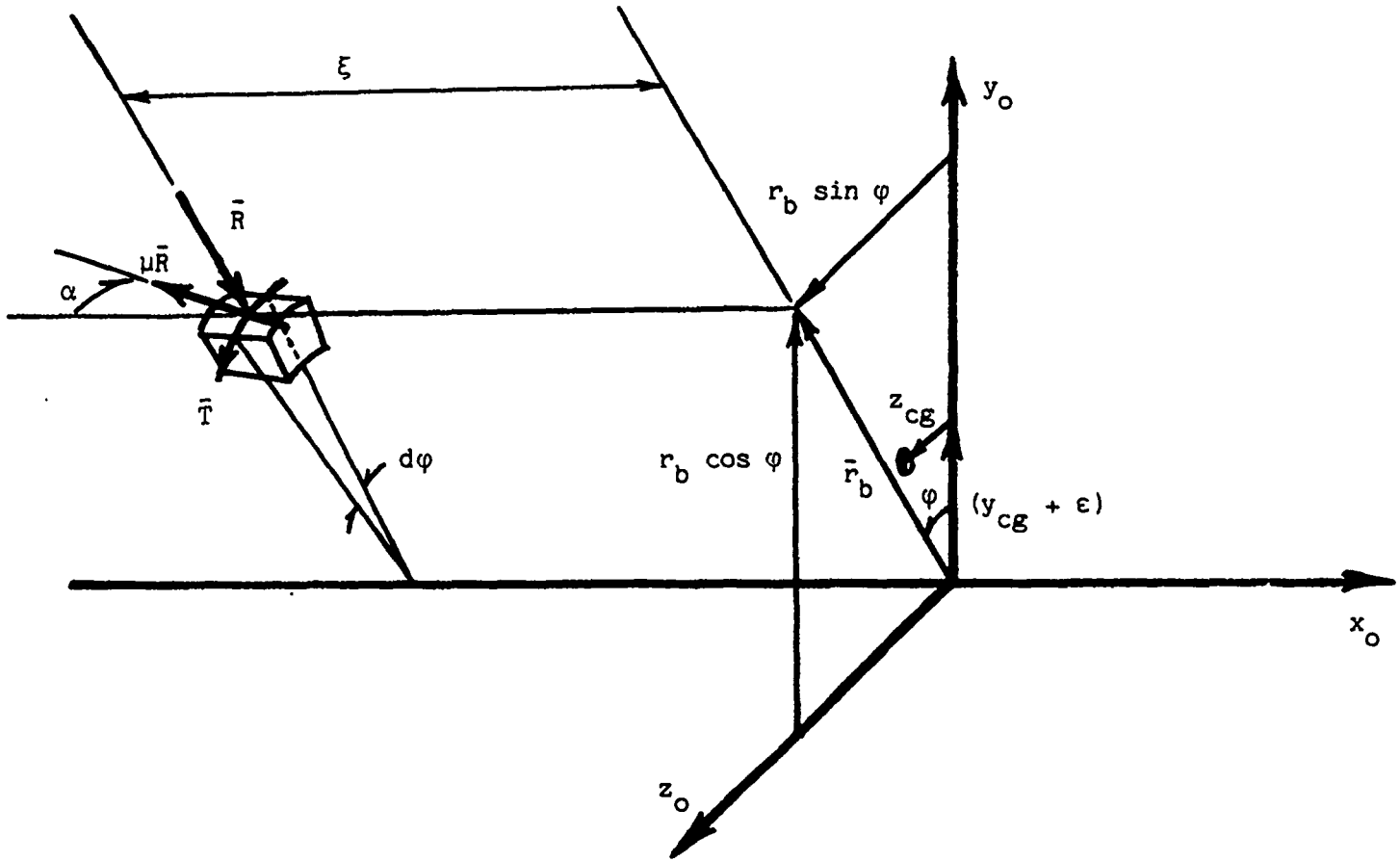

Figure 4 - Loading on Typical Differential Element of Rotating Band

$$
\left.
\begin{aligned}
F^c_{x_o} &= -2\pi r_b \mu k' \delta_o \cos\alpha \\
F^c_{y_o} &= \pi r_b k' \left\{(\ell_b - \tfrac{h}{2})\psi - y_{cg} + \mu \sin\alpha \left[z_{cg} + (\ell_b - \tfrac{h}{2})\vartheta\right]\right\} \\
F^c_{z_o} &= -\pi r_b k' \left\{z_{cg} + (\ell_b - \tfrac{h}{2})\vartheta + \mu \sin\alpha \left[y_{cg} - (\ell_b - \tfrac{h}{2})\psi\right]\right\}
\end{aligned}
\right\} \qquad (58)
$$

where ℓ_b denotes the distance from the projectile c.g. to the rear face of the rotating band (which is assumed to be located aft of the c.g.), h denotes the width of the rotating band, and k' (= k h) denotes the "spring" stiffness of the rotating band per unit circumferential length.

Referring again to Figure 4, the moment arm, $\bar{\ell}_M$, from the projectile c.g. to the load acting on the differential element is given by

$$
\bar{\ell}_M = -\xi\,\hat{i}_o + \left[r_b \cos\varphi - (y_{cg} + \varepsilon)\right]\hat{j}_o + \left[r_b \sin\varphi - z_{cg}\right]\hat{k}_o \ . \qquad (59)
$$

Hence, the resultant moment applied to the projectile c.g. is given by

$$
\bar{M} = \iint_{S_b} \bar{\ell}_M \times d\bar{F}_c \qquad (60)
$$

where S_b denotes the instantaneous rotating-band/bore interfacial surface area.

Substituting equations (56), (57) and (59) into equation (60), and performing the indicated integration, there results the contribution to the moment components acting at the projectile c.g. (relative to S_o) due to rotating band contact with the bore, as follows

$$
\left.
\begin{aligned}
M^c_{x_o} &= r_b \left[2\pi r_b h T - \tan\alpha\, F^c_{x_o}\right] + z_{cg} F^c_{y_o} - (y_{cg} + \varepsilon) F^c_{z_o} \\
M^c_{y_o} &= -z_{cg} F^c_{x_o} + (\ell_b - \tfrac{h}{2}) F^c_{z_o} - \pi r_b^2 k' \mu \cos\alpha \left[z_{cg}\right. \\
&\quad \left. + (\ell_b - \tfrac{h}{2})\vartheta\right] + \frac{\pi r_b h^2 k'}{12}\left[(\mu \sin\alpha)\psi - \vartheta\right] \\
M^c_{z_o} &= (y_{cg} + \varepsilon) F^c_{x_o} - (\ell_b - \tfrac{h}{2}) F^c_{y_o} + \pi r_b^2 k' \mu \cos\alpha \left[y_{cg}\right. \\
&\quad \left. - (\ell_b - \tfrac{h}{2})\psi\right] - \frac{\pi r_b h^2 k'}{12}\left[\psi + (\mu \sin\alpha)\vartheta\right]
\end{aligned}
\right\} \qquad (61)
$$

where $F^c_{x_o}$, $F^c_{y_o}$ and $F^c_{z_o}$ are as defined in equation (58), and $T \equiv 0$ for a smoothbore application.

Referring to equation (61), it is of interest to note that characterization of the elastic response of the rotating band by a Winkler foundation model gives rise to the so called "foundation" moment, which manifests itself via the last term on the right-hand sides of the expressions for $M^c_{y_o}$ and $M^c_{z_o}$.

The desired contribution to the moment components M_x, M_y and M_z written relative to S for application to equation (36), is obtained applying the inverse of the transformation given in equation (22), from which there results (noting Assumption (viii))

$$\left.\begin{aligned} M^c_x &= M^c_{x_o} + \psi M^c_{y_o} - \vartheta M^c_{z_o} \\ M^c_y &= M^c_{y_o} - \psi M^c_{x_o} \\ M^c_z &= M^c_{z_o} + \vartheta M^c_{x_o} \end{aligned}\right\} . \qquad (62)$$

2.3.3 Bourrelet/Bore Interfacial Contact Loading

To accommodate a variety of bourrelet designs, we distinguish between bourrelets which are initially either bore diameter or greater, or sub-caliber. In either case, to facilitate computations allowing for bourrelet/bore contact, the instantaneous curvature of the gun tube axis between the planes containing the rear face of the rotating band and the forward face of the bourrelet is neglected.

Considering the case wherein the bourrelet is either bore diameter or greater, it is treated as was the rotating band in the preceding section. Hence, the equations developed in the preceding section and, in particular, equations (58), (61) and (62), with ℓ_b replaced by the negative of the distance from the projectile c.g. to the forward face of the bourrelet (assuming the bourrelet is forward of the projectile c.g.), h replaced by the width of the bourrelet, and μ and k' replaced by appropriate values for the bourrelet remain valid for this case.

Considering the case wherein the bourrelet is sub-caliber, we accommodate bourrelet impact with the bore by applying the principles of linear and angular

momentum (in integrated form) to determine the impulsive motions imparted to the projectile during impact. It is noted that at the instant of impact an impulsive load, $\hat{\bar{F}}$, is generated at the bourrelet/bore interface and, in addition, since projectile spin is constrained by the rifling twist in the rifled bore application, an impulsive torque, $\hat{\bar{T}}$, is simultaneously generated at the rotating-band/bore interface.

Letting $\Delta(\ )$ denote the "jump" (sudden increment) in the parameter $(\ )$ due to impact, the principle of linear momentum (integrated with respect to time) may be written in the form

$$m_p \, \Delta\bar{v}'_{cg} = \hat{\bar{F}} \tag{63}$$

where $\bar{v}'_{cg}$ denotes the velocity of the projectile c.g. relative to the gun tube.

Similarly, the principle of angular momentum (integrated with respect to time) may be written in the form

$$\Delta\bar{H} = \bar{r}_1 \times \hat{\bar{F}} + \hat{\bar{T}} \tag{64}$$

where $\bar{H}$ denotes the angular momentum of the projectile about its c.g. and $\bar{r}_1$ denotes the position vector from the projectile c.g. to the point of application of the impulsive load.

Referring to Figure 5 and the notation introduced in Section 2.1

$$\left.\begin{aligned}
\hat{\bar{F}} &= -[\mu_1 \cos\alpha]\,\hat{R}\,\hat{i}_o - [\cos\varphi_1 - \mu_1 \sin\alpha \sin\varphi_1]\,\hat{R}\,\hat{j}_o \\
&\quad - [\sin\varphi_1 + \mu_1 \sin\alpha \cos\varphi_1]\,\hat{R}\,\hat{k}_o \\
\hat{\bar{T}} &= \begin{cases} -\hat{T}\,\hat{i}_o \ ; & \text{rifled bore} \\ 0 \ ; & \text{smoothbore} \end{cases} \\
\bar{r}_1 &= \ell_1\,\hat{i}_o + [r_b \cos\varphi_1 - (y_{cg} + \varepsilon)]\,\hat{j}_o + [r_b \sin\varphi_1 - z_{cg}]\,\hat{k}_o
\end{aligned}\right\} \tag{65}$$

where $\hat{R}$ denotes the radially directed impulsive load acting at the bourrelet/bore interface, $\hat{T}$ denotes the circumferentially directed impulsive torque acting

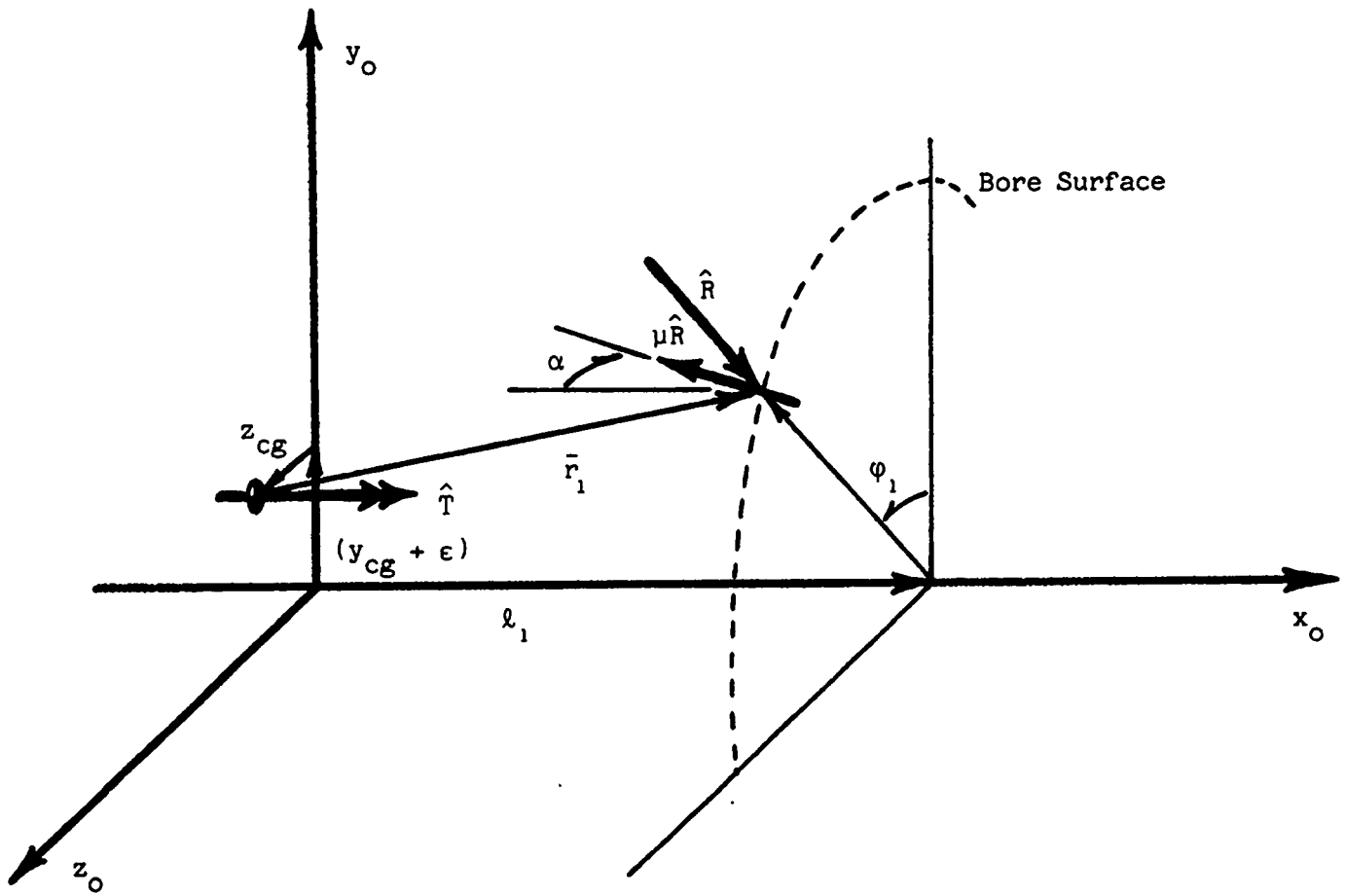

Figure 5 - Bourrelet/Bore Impact Loading

at the rotating-band/bore interface, μ_1 denotes the friction coefficient at the bourrelet/bore interface, α is as defined in equation (55), and ℓ_1 and φ_1 are as depicted.

Referring again to the notation of Section 2.1 and, in addition, assuming the validity of equation (37), it may be shown that

$$\left.\begin{aligned} \bar{v}'_{cg} &= v_p\,\hat{i}_o + [\dot{y}_{cg} - z_{cg}\,\dot{\varphi}_o]\,\hat{j}_o + [\dot{z}_{cg} + (y_{cg} + \varepsilon)\,\dot{\varphi}_o]\,\hat{k}_o \\ \bar{H} &= I_{xx}\,(\dot{\varphi}_o + \psi\,\dot{\vartheta} - \vartheta\,\dot{\psi})\,\hat{i} + I_{yy}\,(\dot{\vartheta} - \psi\,\dot{\varphi}_o)\,\hat{j} + I_{zz}\,(\dot{\psi} + \vartheta\,\dot{\varphi}_o)\,\hat{k} \end{aligned}\right\} \quad (66)$$

Substituting equations (65) and (66) into equations (63) and (64), performing the indicated vector operation on the right-hand side of equation (64) and, furthermore, transforming the resulting expressions from S_o to S (noting equation (37)), there results the six scalar equations

$$\left.\begin{aligned} m_p\,\Delta v_p &= -\,(\mu_1 \cos\alpha)\,\hat{R} \\ m_p\,(\Delta\dot{y}_{cg} - z_{cg}\,\Delta\dot{\varphi}_o) &= (-\cos\varphi_1 + \mu_1 \sin\alpha \sin\varphi_1)\,\hat{R} \\ m_p\,[\Delta\dot{z}_{cg} + (y_{cg} + \varepsilon)\,\Delta\dot{\varphi}_o] &= -\,(\sin\varphi_1 + \mu_1 \sin\alpha \cos\varphi_1)\,\hat{R} \\ I_{xx}\,(\Delta\dot{\varphi}_o + \psi\,\Delta\dot{\vartheta} - \vartheta\,\Delta\dot{\psi}) &= \hat{R}\,\{\varepsilon \sin\varphi_1 + \mu_1 \sin\alpha\,[(y_{cg} + \varepsilon \\ &\quad - \ell_1\,\psi)\cos\varphi_1 + (z_{cg} - \ell_1\,\vartheta)\sin\varphi_1 - r_b] - \mu_1 \cos\alpha \\ &\quad \times [r_b\,(\psi \sin\varphi_1 + \vartheta \cos\varphi_1) - \varepsilon\,\vartheta]\} - \hat{T} \\ I_{yy}\,(\Delta\dot{\vartheta} - \psi\,\Delta\dot{\varphi}_o) &= \hat{R}\,\{(\ell_1 - \varepsilon\,\psi)\sin\varphi_1 + \mu_1 \sin\alpha[(\ell_1 - \varepsilon\,\psi) \\ &\quad \times \cos\varphi_1 + r_b\,\psi] - \mu_1 \cos\alpha\,(r_b \sin\varphi_1 - z_{cg})\} + \psi\,\hat{T} \\ I_{zz}\,(\Delta\dot{\psi} + \vartheta\,\Delta\dot{\varphi}_o) &= R\,\{-\ell_1 \cos\varphi_1 + \varepsilon\,\vartheta \sin\varphi_1 + \mu_1 \sin\alpha \\ &\quad \times (\ell_1 \sin\varphi_1 + \varepsilon\,\vartheta \cos\varphi_1 - r_b\,\vartheta) + \mu_1 \cos\alpha\,[r_b \cos\varphi_1 \\ &\quad - (y_{cg} + \varepsilon)]\} - \vartheta\,\hat{T} \end{aligned}\right\} \quad (67)$$

with $\hat{T} \equiv 0$ in the smoothbore application.

In addition, the constraint imposed by the rifling, namely equation (14), requires that

$$\Delta\dot{\varphi}_o = t_w \, \Delta v_p \quad . \tag{68}$$

Hence, considering the rifled bore application, equations (67) and (68) represent seven algebraic equations in the eight unknowns, Δv_p, $\Delta\dot{y}_{cg}$, $\Delta\dot{z}_{cg}$, $\Delta\dot{\varphi}_o$, $\Delta\dot{\vartheta}$, $\Delta\dot{\psi}$, $\hat{R}$, and $\hat{T}$; whereas, considering the smoothbore application, equation (67) contains seven unknowns. The remaining equation required to complete the set for either application is obtained by characterizing the impact process at the bourrelet/bore interface via introduction of the coefficient of restitution, e.

In accordance with the above notation and assumptions, the velocity relative to the bore of the point on the bourrelet which impacts the bore is given by

$$\begin{aligned}\bar{v}_c' = {} & \{v_p + (r_b \sin\varphi_1 - z_{cg})\,\dot{\vartheta} - [r_b \cos\varphi_1 - (y_{cg} + \varepsilon)]\,\dot{\psi}\}\,\hat{i}_o \\ & + \{\dot{y}_{cg} + \ell_1\,\dot{\psi} - r_b\,\dot{\varphi}_o \sin\varphi_1\}\,\hat{j}_o + \{\dot{z}_{cg} - \ell_1\,\dot{\vartheta} \\ & + r_b\,\dot{\varphi}_o \cos\varphi_1\}\,\hat{k}_o \quad .\end{aligned} \tag{69}$$

Since compression and restitution during impact occur in a direction normal to the bore surface (along the line of action of $\hat{R}$), the component of $\bar{v}_c'$ normal to the bore surface immediately following restitution, namely $(\bar{v}_c' \cdot \hat{i}_r)^+$, is related to its value just prior to impact, namely $(\bar{v}_c' \cdot \hat{i}_r)^-$, via the coefficient of restitution, that is

$$(\bar{v}_c' \cdot \hat{i}_r)^+ = -\,e\,(\bar{v}_c' \cdot \hat{i}_r)^- \quad . \tag{70}$$

Hence, there results from equations (69) and (70)

$$\begin{aligned}(\Delta\dot{y}_{cg} + \ell_1\,\Delta\dot{\psi})\cos\varphi_1 + (\Delta\dot{z}_{cg} - \ell_1\,\Delta\dot{\vartheta})\sin\varphi_1 = {} & (1 + e) \\ \times [(\dot{y}_{cg}^- + \ell_1\,\dot{\psi}^-)\cos\varphi_1 + (\dot{z}_{cg}^- - \ell_1\,\dot{\vartheta}^-)\sin\varphi_1] \quad .\end{aligned} \tag{71}$$

Equations (67), (68) and (71) in the rifled bore application, and equations (67) and (71) in the smoothbore application, completely prescribe the "jump" conditions at impact in terms of projectile orientation and motion just prior to impact and the relative material properties of the bourrelet (via the coefficient of restitution). It is noted once again that, in general, bourrelet impact with the bore gives rise to non-zero increments in the parameter $\dot{\varphi}_o$ for both rifled and smoothbore applications.

2.3.4 Propellant Gas Pressure and Compressed Air Loadings

The loads and moments applied to the projectile c.g. due to propellant gas pressure acting at the base of the projectile and "ram" (compressed) air ahead of the projectile are derived subject to the following assumptions:

(i) *both the projectile base and "ram" air pressures are assumed to be known functions of time only, and at any instant are uniformly distributed over the respective projectile surfaces over which they act;*

(ii) *for cases wherein the bourrelet is either bore diameter or greater, both the rotating band and bourrelet are assumed to act as ideal gas seals; for cases wherein the bourrelet is sub-caliber, the rotating band alone is assumed to act as an ideal gas seal;*

(iii) *the Euler angles ψ and ϑ satisfy equation (37).*

It follows from Assumption (i) that the base and "ram" air pressures act as effective hydrostatic pressures; generating a force equal to $-(p\ dA)\ \hat{i}_n$ acting on a differential surface area element, dA, with unit outward normal $\hat{i}_n$. Further, from general principles of hydrostatics and Assumption (ii), these pressure loadings may be replaced by resultant forces acting at the geometric center of, and directed perpendicular to, the sealing planes.

Considering first cases wherein the bourrelet is either bore diameter or greater, the sealing planes contain the forward face of the bourrelet and the rear face of the rotating band. Hence, the points of application of the resultant pressure loads are defined by the respective intersection of each of these planes with the gun tube centerline, as depicted in Figure 6.

Referring to Figure 6, and noting that since $\hat{i}$ is parallel to the geometric axis of the projectile, it follows that

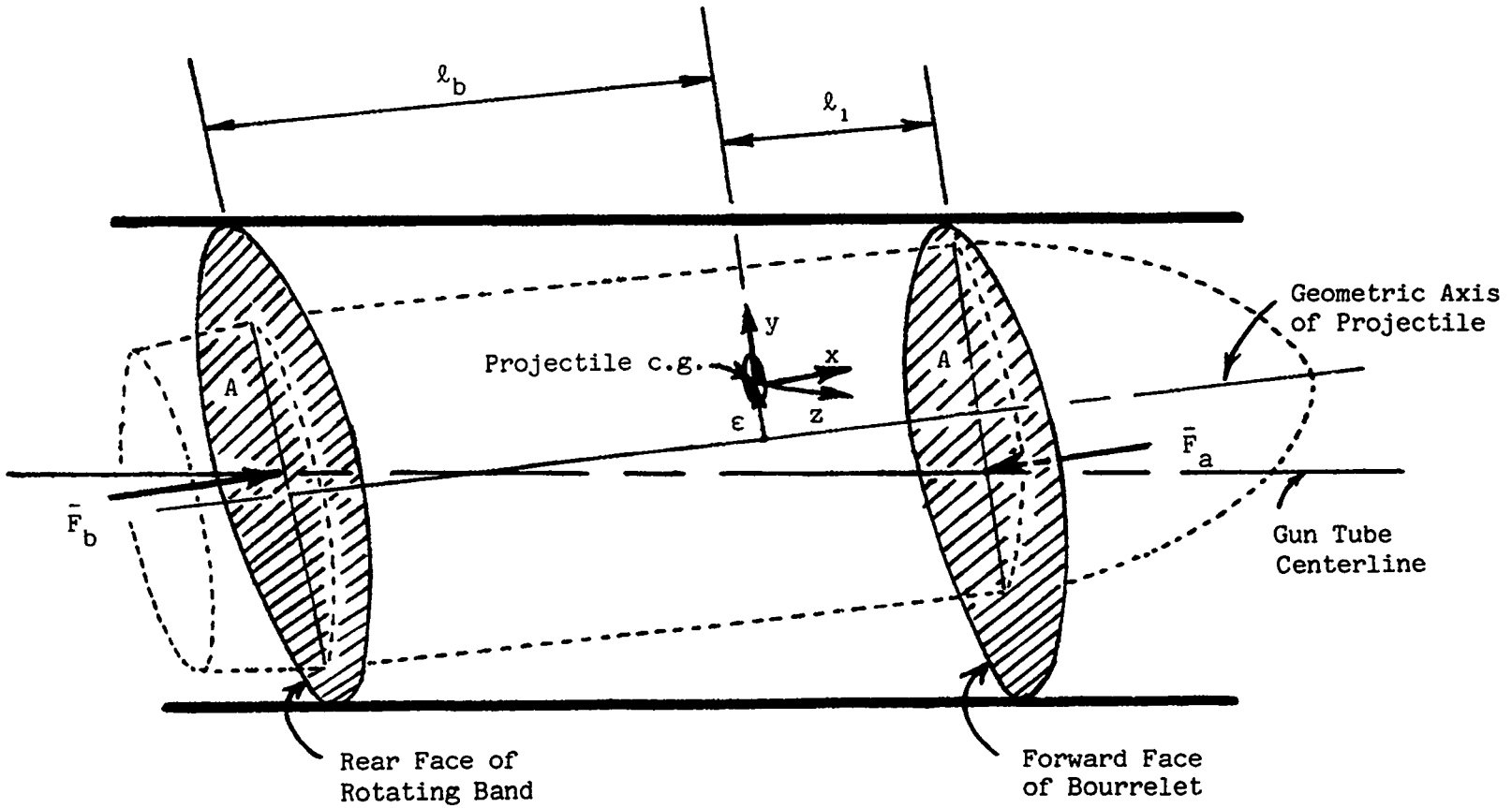

Figure 6 - Projectile Base and "Ram" Air Pressure Loads

$$\left.\begin{aligned} \bar{F}_a &= - p_a A \hat{i} \\ \bar{F}_b &= p_b A \hat{i} \end{aligned}\right\} \tag{72}$$

where p_a and p_b denote respectively the instantaneous "ram" air and projectile base pressures, and A denotes the projected area of the bourrelet and rotating band planes perpendicular to $\hat{i}$.

Under Assumption (iii), it follows that

$$A \approx \pi r_b^2 \ . \tag{73}$$

Hence, the resultant pressure load, $\bar{F}_p$, is given by

$$\bar{F}_p = \pi r_b^2 (p_b - p_a) \hat{i} \tag{74}$$

which is written relative to S_o for application to equation (35) in the form

$$\bar{F}_p = F^p_{x_o} \hat{i}_o + F^p_{y_o} \hat{j}_o + F^p_{z_o} \hat{k}_o \tag{75}$$

where (noting Assumption (iii)),

$$\left.\begin{aligned} F^p_{x_o} &= \pi r_b^2 (p_b - p_a) \\ F^p_{y_o} &= \pi r_b^2 (p_b - p_a) \psi \\ F^p_{z_o} &= \pi r_b (p_b - p_a) \vartheta \end{aligned}\right\} . \tag{76}$$

Once again in view of Assumption (iii), the moment arm, $\bar{\ell}_a$, from the projectile c.g. to the "ram" air load, $\bar{F}_a$, is given by

$$\bar{\ell}_a = \ell_1 \hat{i} - (y_{cg} + \varepsilon + \ell_1 \psi) \hat{j} - (z_{cg} - \ell_1 \vartheta) \hat{k} \tag{77}$$

where ℓ_1 denotes the distance from the projectile c.g. to the forward face of the bourrelet.

The corresponding moment arm, $\bar{\ell}_b$, to the load $\bar{F}_b$ is given by

$$\bar{\ell}_b = - \ell_b \hat{i} - (y_{cg} + \epsilon - \ell_b \psi) \hat{j} - (z_{cg} + \ell_b \vartheta) \hat{k} \tag{78}$$

where ℓ_b, as previously defined, denotes the distance from the projectile c.g. to the rear face of the rotating band.

Hence, the resultant moment applied to the projectile c.g. is given by

$$\bar{M}_p = \bar{\ell}_a \times \bar{F}_a + \bar{\ell}_b \times \bar{F}_b \ . \tag{79}$$

Substituting equations (72), (77) and (78) into equation (79), and performing the indicated vector operations, there results the desired contribution to the moment components acting at the projectile c.g. (relative to S) due to propellant gas and "ram" air pressures, in the form

$$\left.\begin{aligned} M_x^p &= 0 \\ M_y^p &= - \pi r_b^2 [(p_b - p_a) z_{cg} + \vartheta (p_b \ell_b + p_a \ell_1)] \\ M_z^p &= \pi r_b^2 [(p_b - p_a) (y_{cg} + \epsilon) - \psi (p_b \ell_b + p_a \ell_1)] \end{aligned}\right\} . \tag{80}$$

Considering the case wherein the bourrelet is sub-caliber, equation (76) remains unchanged, while equation (80) is modified by replacing ℓ_1 by $- (\ell_b - h)$; where h, as previously defined, denotes the width of the rotating band.

2.4 Solution Technique

Summing corresponding force components from equations (47), (58) and (76), there results for application to equation (35)

$$\left.\begin{aligned} F_{x_o} &= F^w_{x_o} + F^c_{x_o} + F^p_{x_o} \\ F_{y_o} &= F^w_{y_o} + F^c_{y_o} + F^p_{y_o} \\ F_{z_o} &= F^w_{z_o} + F^c_{z_o} + F^p_{z_o} \end{aligned}\right\} . \tag{81}$$

Similarly, summing corresponding moment components from equations (62) and (80), there results for application to equation (36)

$$\left.\begin{aligned} M_x &= M_x^c \\ M_y &= M_y^c + M_y^p \\ M_z &= M_z^c + M_z^p \end{aligned}\right\} . \qquad (82)$$

Within the framework of the assumptions introduced, equations (14), (35) and (36), with the applied loads and moments as defined in equations (81) and (82), and the projectile "jump" conditions due to bourrelet/bore impact as defined in equations (67), (68) and (71), constitute the desired formulation for a rifled bore gun tube; whereas, deleting equations (14) and (68), there results the desired formulation for a smoothbore gun tube.

Considering either formulation, it is seen that projectile in-bore motion is prescribed in terms of projectile design data, interior ballistics data, and gun tube design and motion data. Of these data, gun tube motion is generally not known a priori. In fact, an objective of this formulation is to define the mutual effects of projectile/gun-tube interaction. Hence, to satisfy this objective, the formulation herein developed (for both rifled and smoothbore firings) is to be solved simultaneously with a compatible gun dynamics simulation, such as DYNACODE-G. In addition, since the onset of bourrelet/bore impact is also generally not known a priori, the solution technique requires monitoring projectile in-bore motion at each instant to determine such onset and, accordingly, introduction of the projectile "jump" conditions.

SECTION 3

COMPARISON WITH OTHER PROJECTILE MOTION FORMULATIONS

The formulation developed in Section 2 is general in that it prescribes the full six degree-of-freedom motion of a projectile of finite geometry and inertia traveling in a flexible (rifled or smoothbore) gun tube. The degrees-of-freedom selected correspond to three independent translational motions of the projectile c.g. relative to the gun tube axis and three independent rotations of the projectile about its c.g. (corresponding to pitch, yaw and roll motions). In addition, the formulation accommodates bourrelet impact and rebound with the bore (via impulsive loadings which give rise to "jump" conditions in projectile motion parameters during impact). Finally, since gun tube motion (which is unrestricted in this formulation) is generally not known a priori, the projectile equations of motion have been formulated with the intent of being solved simultaneously with the equations of a compatible gun dynamics simulation, such as DYNACODE-G.

A similar, but far more restrictive formulation has recently been presented by S.H. Chu (Ref. 3). Chu permits the projectile three degrees-of-freedom; two orthogonal translational motions of the projectile c.g. relative to the gun tube and one rotational (pitching) motion. As a consequence of neglecting the remaining degrees-of-freedom, the gun tube centerline, the projectile c.g., and the resultants of the rotating band and bourrelet contact load distributions with the bore all lie in the same plane. Hence, Chu's formulation is essentially planar; whereas, the formulation herein presented is of general three-dimensional character.

Another recent, but also restrictive projectile motion formulation has been presented by H.L. Langhaar and A.P. Boresi (Ref. 4). Langhaar and Boresi present a rigorous kinematical description of a point moving along a time-dependent space curve. The point is identified with the geometric center of a rigid projectile; the time-dependent space curve is identified with the centerline of a flexible gun tube. The rigid projectile is further characterized such that its geometric center and c.g. coincide (which precludes the ability to investigate the effects of mass eccentricity), and such that its geometric axis is directed along the instantaneous tangent to the gun tube centerline (which precludes the ability to investigate the effects of projectile pitch and yaw motions relative to the gun tube). The projectile is permitted two degrees-

of-freedom relative to the gun tube; translational motion of its c.g. along the gun tube centerline and rotational motion about the centerline (corresponding to projectile spin). Accounting for rotary inertia of the projectile about its spin axis, there results a traveling point-mass projectile load with superposed gyroscopic couple.

J.J. Wu (Ref. 5) also adopts a traveling point-mass projectile description, but with superposed traveling pitching moment due to mass eccentricity (while neglecting rotary inertia about the pitch axis). Several other investigators (Refs. 6 thru 8) have adopted the simpler traveling point-mass description, with and without mass eccentricity and projectile spin (while neglecting rotary inertia about the spin axis).

SECTION 4

CORRELATION WITH EXPERIMENTAL DATA

Before incorporating the formulation herein developed within DYNACODE-G, it was deemed prudent to verify its validity on its own merits. However, to achieve such verification required establishing an experimental data base, as well as programming the model equations.

To establish the experimental data base, Mr. James O. Pilcher II and Dr. James N. Walbert of the Mechanics and Structures Branch, Interior Ballistics Laboratory, U.S. Army Ballistic Research Laboratory, provided in-bore radar doppler data for firings of two distinct projectile designs from a specially configured 37mm weapon. Miss Susan A. Coates of the Mechanics and Structures Branch accomplished digital conversion of the analog data at the Laboratory Experimental Research Facility of the Interior Ballistics Division of BRL. Descriptions of the projectile designs, test weapon and data base generated are presented in Section 4.1.

A computer program was developed for the specific purpose of model correlation. A description of the program and its required inputs is presented in Section 4.2. Results of the correlation effort are presented in Section 4.3; while several general observations are presented in Section 4.4.

4.1 Description of Test Weapon, Ammunition and Data Base

The experimental test weapon consisted of a fully instrumented 37mm rifled gun tube, with a constant twist of 25 calibers per turn and an in-bore projectile travel of 72.5 inches. In order to minimize gun tube motion, the system design incorporated a heavy, fixed collar supported near the muzzle. The test weapon is shown in Figure 7. The two 37mm projectile designs consisted of solid, steel cores with copper rotating bands and sub-caliber, steel bourrelets as shown, along with pertinent data, in Figure 8.

Analog chamber pressure and in-bore radar doppler data were recorded on magnetic tape for all firings conducted. Digital conversion and reduction were accomplished as noted above. Representative rounds for which all required data were available were selected for the purposes of model correlation. Tabular data for the rounds selected, consisting of pressure, displacement and velocity-time histories, were transmitted to S&D Dynamics, Inc.

The selected data consisted of one record for each projectile design whose

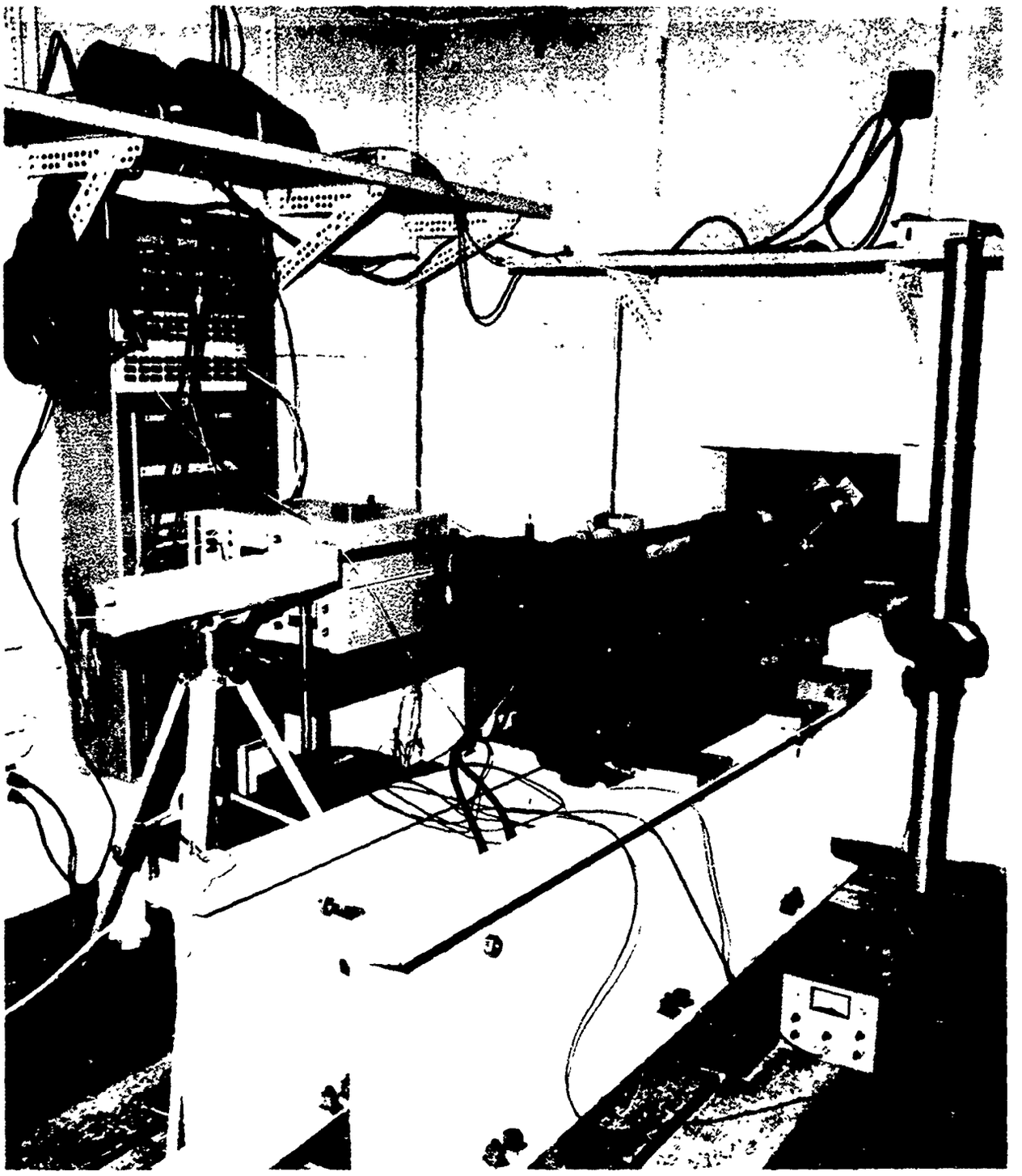

Figure 7 - 37mm Test Weapon (Courtesy BRL)

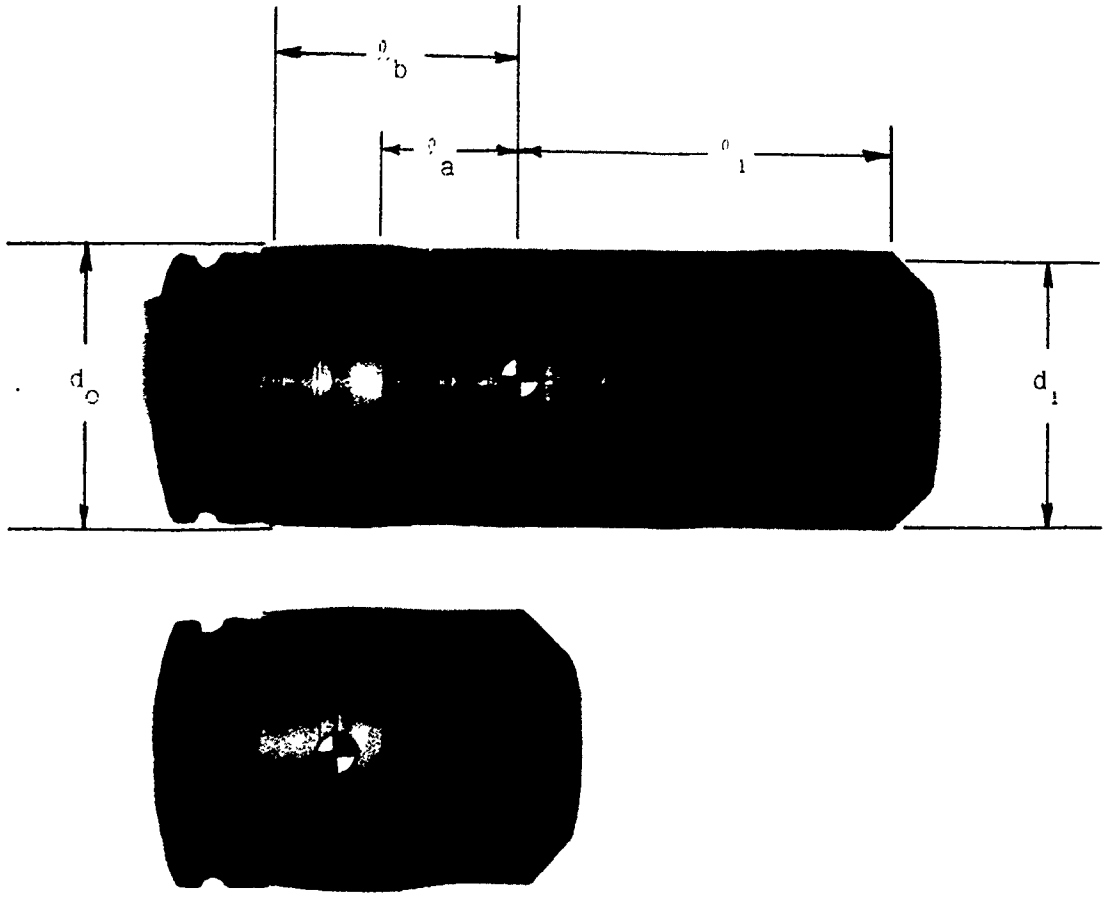

	Long	Short
m_p (lb-sec^2/in)	.0049466	.0026131
ℓ_1 (in)	1.911	.899
ℓ_a (in)	.719	.245
ℓ_b (in)	1.259	.305
d_o (in)	1.506	1.506
d_1 (in)	1.451	1.451

Figure 8 - 37mm Test Projectiles (Courtesy BRL)

frequency-time ("waterfall") plot indicated little or no evidence of balloting, as well as one record for a short round whose "waterfall" plot indicated balloting. As shown in Figure 9, which represents a portion of the latter "waterfall" plot, balloting is indicated by the presence of secondary peaks just behind the main frequency-ridge (which is directly proportional to the instantaneous projectile velocity along the gun tube axis). It is noted that although the secondary peaks have not as yet been quantified in terms of projectile pitch and yaw motions, it is reasonable to use the time periods between peaks as indications of the frequency of balloting. (Refs. 9, 10)

4.2 Computer Program

For the specific purpose of this correlation, the formulation presented in Section 2 was programmed under the assumption of a rigid, straight gun tube; isolating projectile motion from gun tube motion, in accordance with the objective of the experimental arrangement. The computer program, written in MBASIC, was debugged and executed on an Apple II+™ computer, with CP/M™ operating system. With reference to Section 2, the general equations of motion, namely equations (35) and (36), were restructured into a set of simultaneous, nonlinear, first order, ordinary differential equations in the projectile motion parameters, x_p, v_p, y_{cg}, $\dot{y}_{cg}$, z_{cg}, $\dot{z}_{cg}$, ψ, $\dot{\psi}$, ϑ, $\dot{\vartheta}$, and φ_o. This set, with the applied loads and moments defined in Section 2.3, and subject to the above assumption, was integrated via a fourth-order, fixed time-step, Runge-Kutta integration scheme. Additional programming was introduced to detect the onset of bourrelet/bore impact, to apply the "jump" conditions resulting from impact, and to restart the integration scheme following each impact.

Required inputs to the program included geometric and inertia characteristics of the projectile design considered, as indicated in Figure 8, as well as corresponding tabular chamber pressure-time data. Elements of the inertia matrix for each design were hand-calculated based on data supplied. In addition, it was necessary to prescribe the rotating-band "spring" stiffness per unit surface area, k; the coefficients of Coulomb friction at the rotating-band/bore and bourrelet/bore interfaces, namely μ and μ_1 respectively; the instantaneous projectile base pressure, p_b; and, finally, the "ram" air pressure, p_a. In the absence of supplied data for these parameters, additional modeling was undertaken to quantify k, p_b and p_a; whereas, μ and μ_1 were deter-

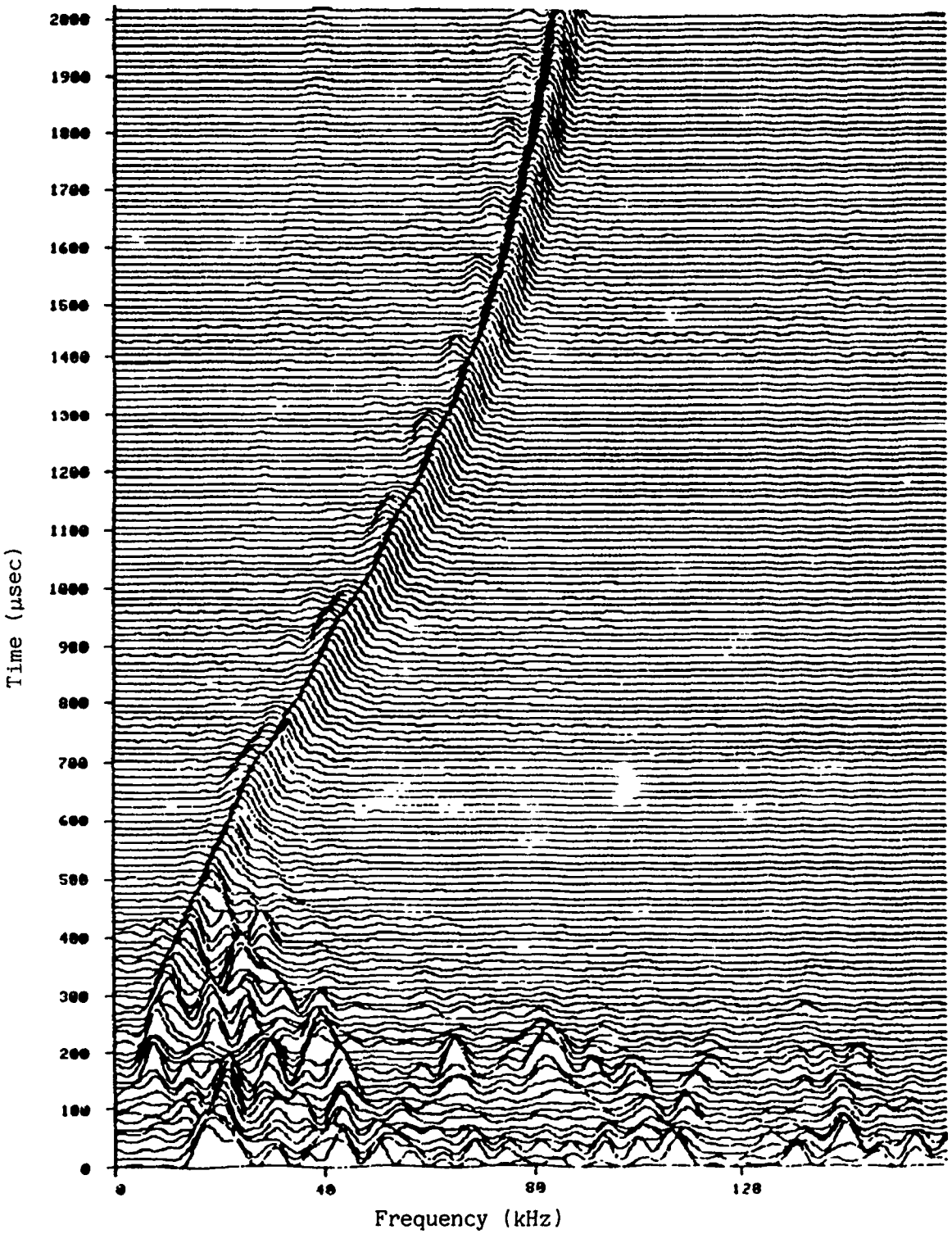

Figure 9 - "Waterfall" Plot for Balloting Round

(Courtesy BRL; BRL Ident. 5)

mined by parametric matching studies.

In accordance with the assumptions introduced in Section 2.3.2, an elastic/plastic analysis of the rotating band, treating the band as a thick-walled tube with plastic boundary initially at the bore interface (Ref. 11), yielded the expression

$$k = E \frac{[(1 + \nu)\, r_o^2 + (1 - \nu)\, r_i^2]}{(1 - \nu^2)\, r_o\, (r_o^2 - r_i^2)} \tag{83}$$

where E denotes Young's modulus for the rotating-band material, ν denotes Poisson's ratio, and r_i and r_o denote respectively the inner and outer band radii. Furthermore, it should be noted that the analysis indicated only a negligible increase in stiffness due to radially inward propagation of the plastic zone for the range of radial displacements anticipated. Hence. the expression for k as given in equation (83) was taken as a constant throughout the in-bore travel.

The instantaneous base pressure, p_b, was prescribed in conventional interior ballistics terms (Ref. 12, for example) as a function of the known chamber pressure, p_c, in the form

$$p_b = \frac{1}{(1 + \frac{c}{2\, m_p})}\, p_c \tag{84}$$

where c denotes the propellant charge.

The "ram" air pressure, p_a, was related to the instantaneous projectile velocity, v_p, via quasi-steady application of the steady state, one-dimensional shock tube relations (Ref. 13), from which there results

$$p_a = \frac{\gamma\, M_p}{4} \left[(\gamma + 1)\, M_p + \sqrt{(\gamma + 1)^2\, M_p^2 + 16}\, \right] p_o \tag{85}$$

where p_o denotes ambient air pressure, γ denotes the specific heat ratio of air and M_p denotes the ratio of projectile speed to ambient air sound speed.

Additional calculated inputs and functional relations required by the program are given in Figure 10. Input to the program is completed by specification of the friction coefficients, μ and μ_1, as defined above, and the orientation of the projectile immediately subsequent to full engraving (defining its

	Long	Short
I_{xx} (in-lb-sec^2)	.020429	.010852
I_{yy} (in-lb-sec^2)	.017378	.006469
I_{zz} (in-lb-sec^2)	.017378	.006469
I_{xy} (in-lb-sec^2)	0	0
I_{xz} (in-lb-sec^2)	0	0
I_{yz} (in-lb-sec^2)	0	0
k (lb/in^3)	1.65064×10^8	1.65064×10^8
δ_o (in)	1.10×10^{-4}	1.10×10^{-4}
p_b (psi)	.940 p_c	.893 p_c
p_a (psi)	$6.8727 \times 10^{-8}\ v_p^2 \left[1 + \sqrt{1 + 4.9908 \times 10^8 / v_p^2}\right]$	

Figure 10 - Additional Required Input

initial state). It is noted that non-zero values of projectile linear and/or angular displacements in its initial state express the amount of misalignment generated during the engraving process. Furthermore, since this "malengraving" entails irreversible plastic flow, elastic restoring forces proportional to these initial displacements do not exist. Consequently, the expressions for the rotating-band/bore interfacial loads and moments are modified within the program by subtracting that portion attributable to the initial state of the projectile.

Program output included instantaneous maximum radial displacements and angular orientations at the rotating band and bourrelet, as well as linear and angular displacements and velocities for all six degrees-of-freedom of the projectile. In addition, bourrelet motion relative to the bore was monitored, with the time of each impact and the magnitude of each impulse output.

4.3 Results of Correlation

For the purpose of quantifying the value of the rotating-band/bore interfacial friction coefficient, μ, a series of program runs were performed for the short round whose experimental record indicated little or no evidence of balloting. Only the value of μ was varied within these runs, all other projectile parameters and initial conditions were held fixed. In addition, since the experimental record did not indicate balloting, the projectile was assumed to have negligible mass eccentricity and misalignment following engraving (i.e., initial linear and angular projectile displacements relative to the bore were assumed to be zero). Output from these runs which prescribe model predictions of projectile displacement and velocity-time histories are presented, along with corresponding experimental data, in Figures 11 and 12, respectively. As may readily be seen from these figures, excellent correlation was achieved for a friction level of $\mu = .05$. Hence, this value was used for all subsequent correlations.

Referring to Figures 11 and 12, it is noted that model output begins immediately subsequent to full engraving. For each round considered, required initial values of projectile displacement and velocity were determined via comparison of experimental data with the known projectile geometry and free-run. Alignment of the chamber pressure-time history and determination of its initial value for each firing were accomplished by graphically matching the

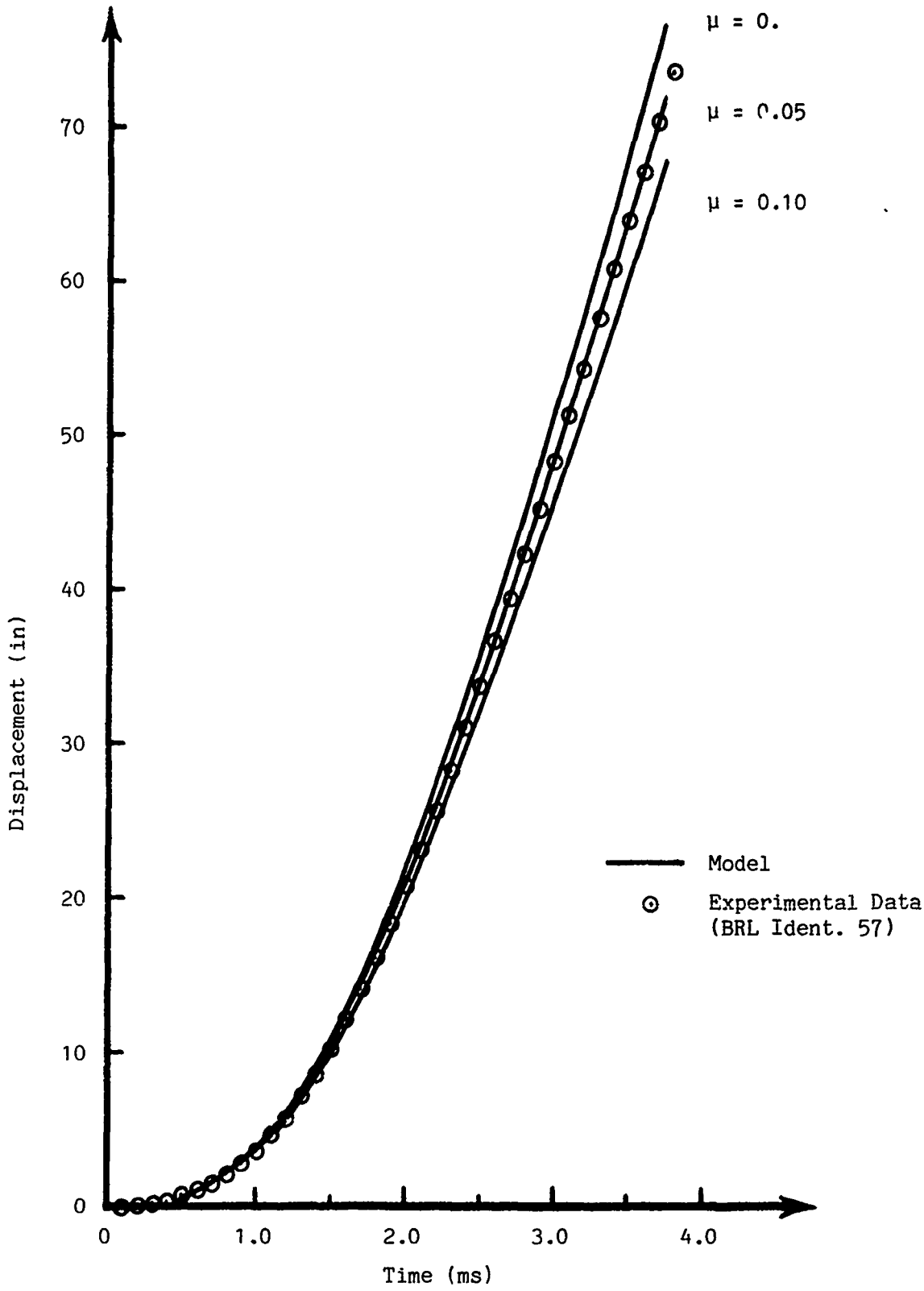

Figure 11 - Displacement-Time Correlation (Short Round w/o Balloting)

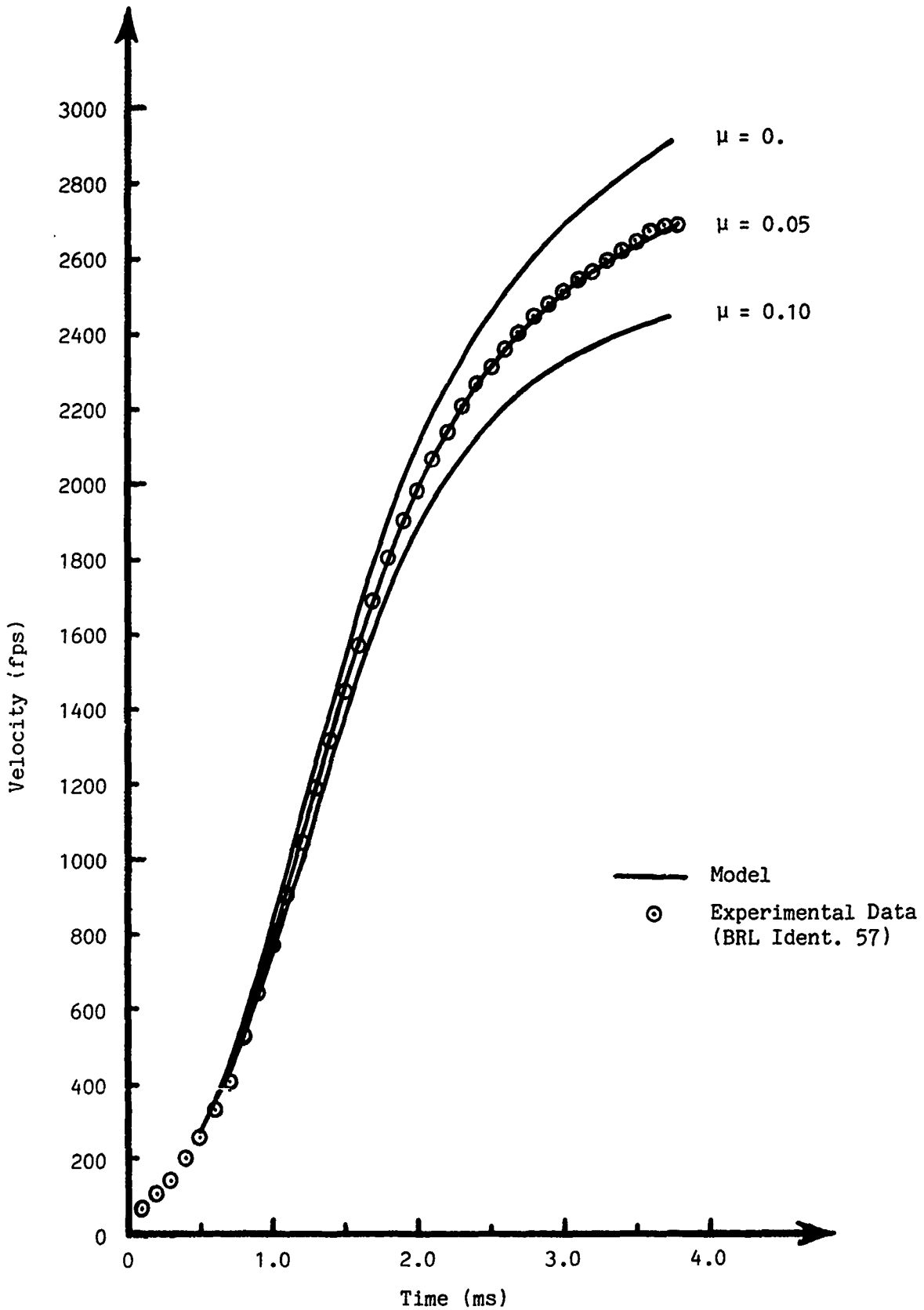

Figure 12 - Velocity-Time Correlation (Short Round w/o Balloting)

pressure-time curve to the projectile acceleration-time curve derived from the experimental velocity record. This procedure was repeated for each round considered.

The program was exercised next for comparison with the experimental record corresponding to the long projectile which also evidenced little or no balloting. Model correlations with experimental data for projectile displacement and velocity-time histories are presented in Figures 13 and 14, respectively. As is seen, excellent theoretical/experimental agreement is obtained for this round using the friction level previously determined.

Considering transverse and/or balloting motion in both of the above cases, model output indicated that (with negligible mass eccentricity and malengraving) the maximum radial displacement of the projectile is of the order of 10^{-8} inches and the maximum yaw and pitch are of the order of 10^{-5} milliradians. Since these values are small compared to the maximum allowable values determined by bourrelet/bore clearance and rotating band thickness, namely, of the order of 10^{-3} inches and 1 milliradian respectively, it is reasonable to conclude that the model correlates well with experimental data regarding balloting motions for both cases considered.

Finally, the model was exercised for the purpose of correlation with the experimental record corresponding to the short round with appreciable evidence of balloting. The model configuration for this correlation included a mass eccentricity of .02 inches and an initial malengraved state characterized by an initial pitch of 3 milliradians. However, it is noted that (to within practical limitations) there exist numerous combinations of eccentricity and/or malengraving which give rise to balloting. The configuration selected resulted in appreciable balloting with multiple bourrelet/bore impacts throughout the in-bore travel, and thereby illustrated the full capabilities of the model. For this case, the coefficient of friction at the bourrelet/bore interface, μ_1, was taken equal to .3 and the coefficient of restitution for impact, e, was taken equal to 1 (rendering perfectly elastic impacts).

As for the two previous rounds considered, theoretical correlation with experimental projectile displacement and velocity-time histories are shown for this balloting round in Figures 15 and 16, respectively. Once again it is seen that excellent theoretical/experimental agreement is achieved in terms of longitudinal projectile motion.

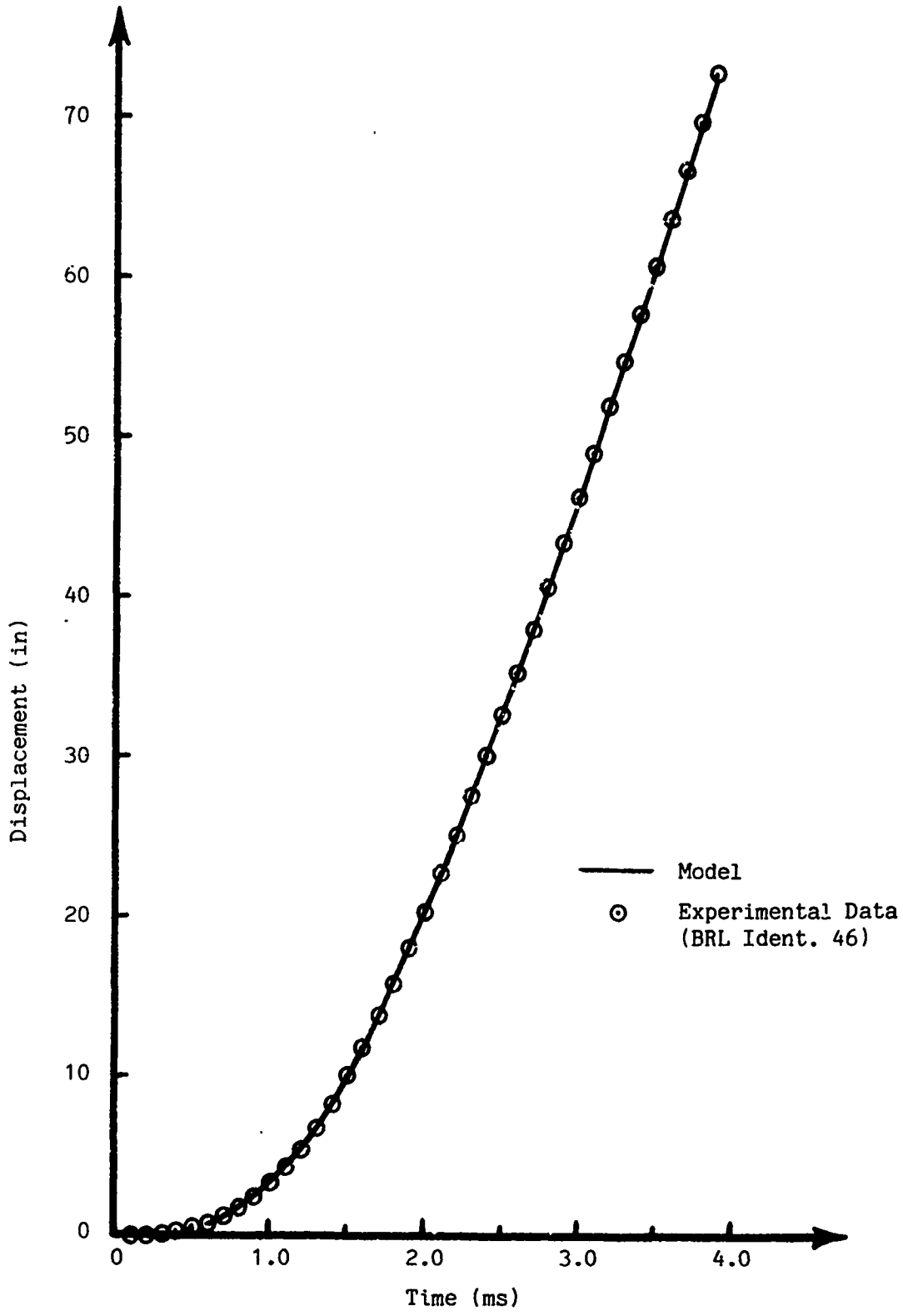

Figure 13 - Displacement-Time Correlation (Long Round w/o Balloting)

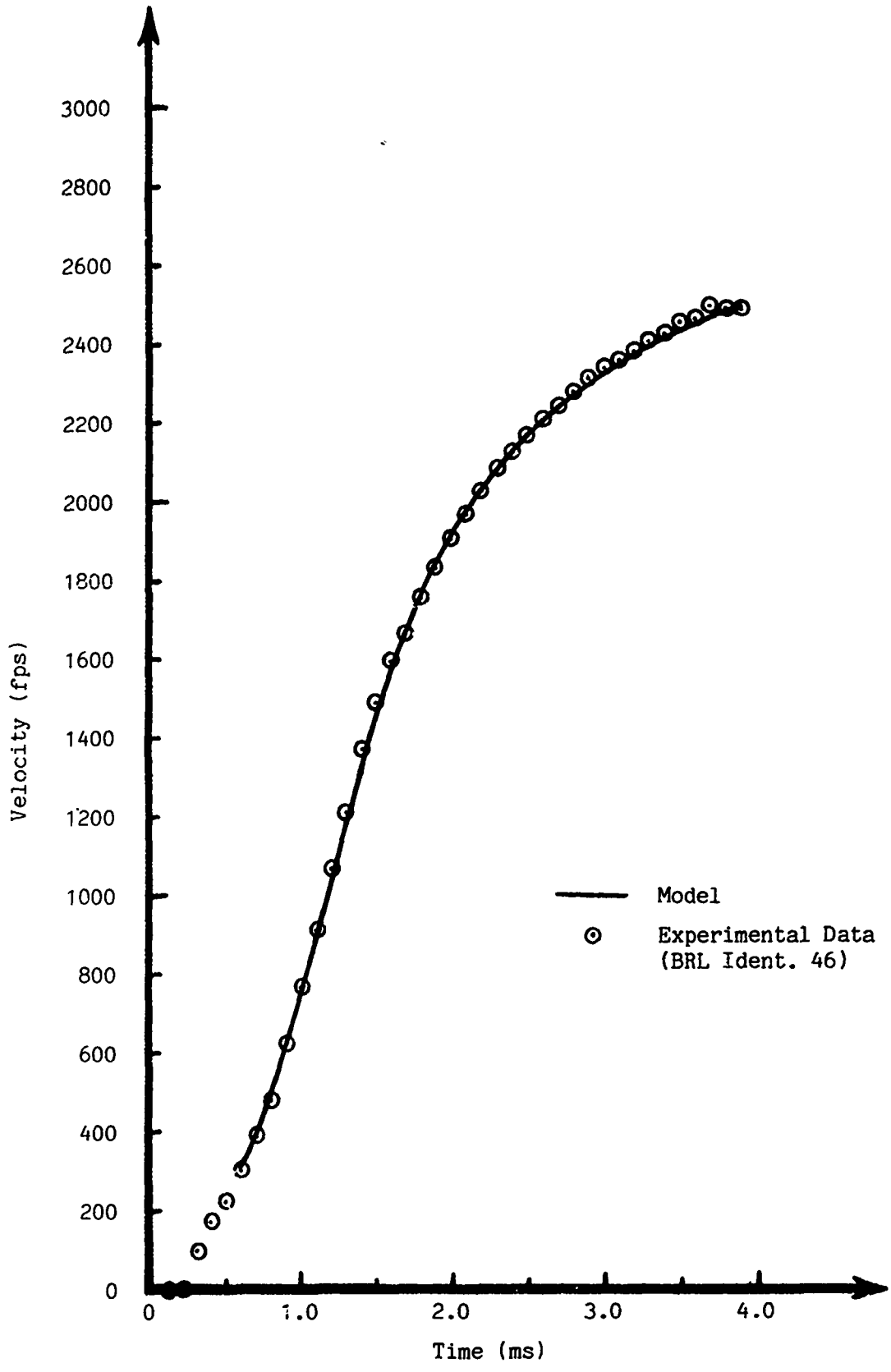

Figure 14 - Velocity-Time Correlation (Long Round w/o Balloting)

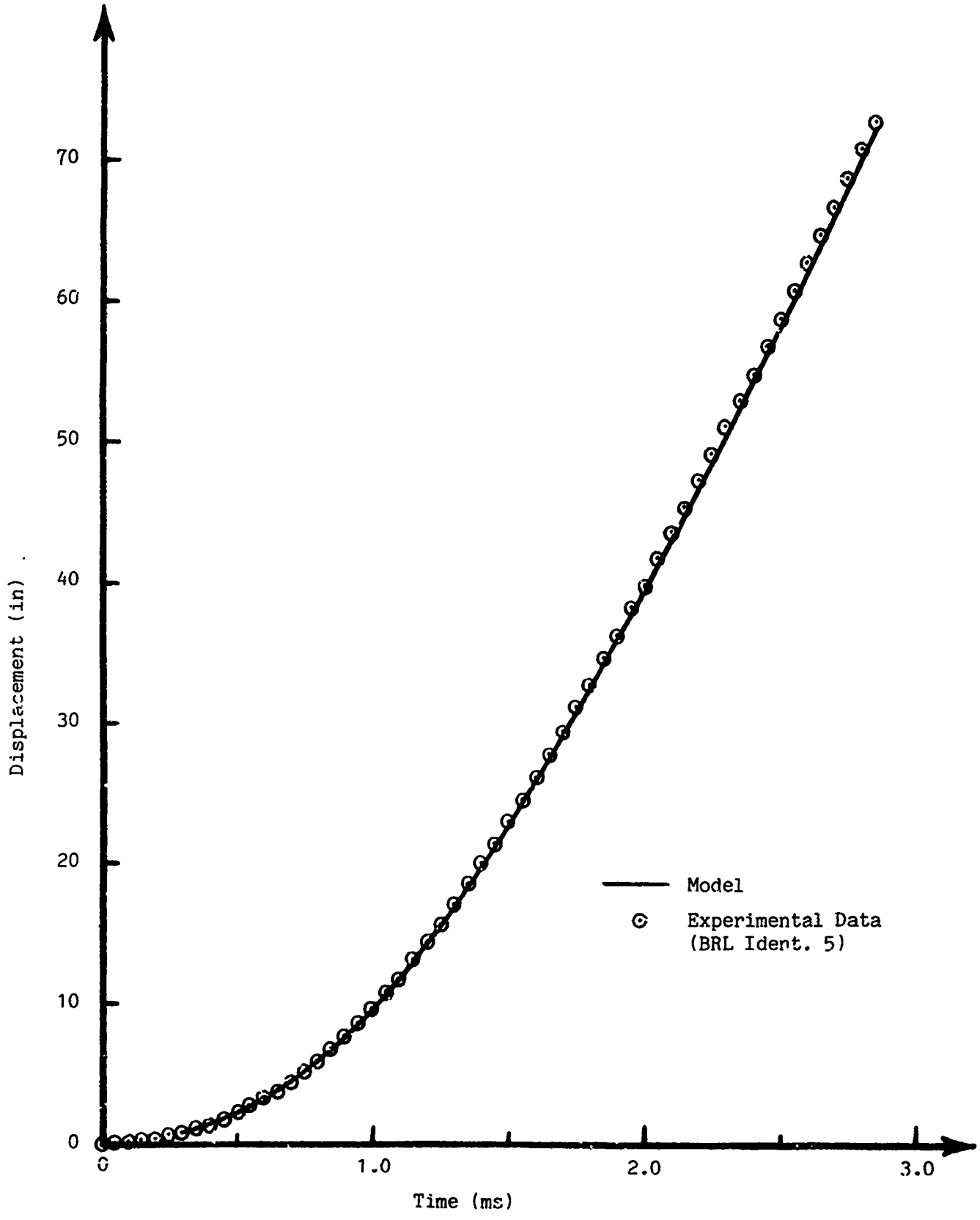

Figure 15 - Displacement-Time Correlation (Short Round with Balloting)

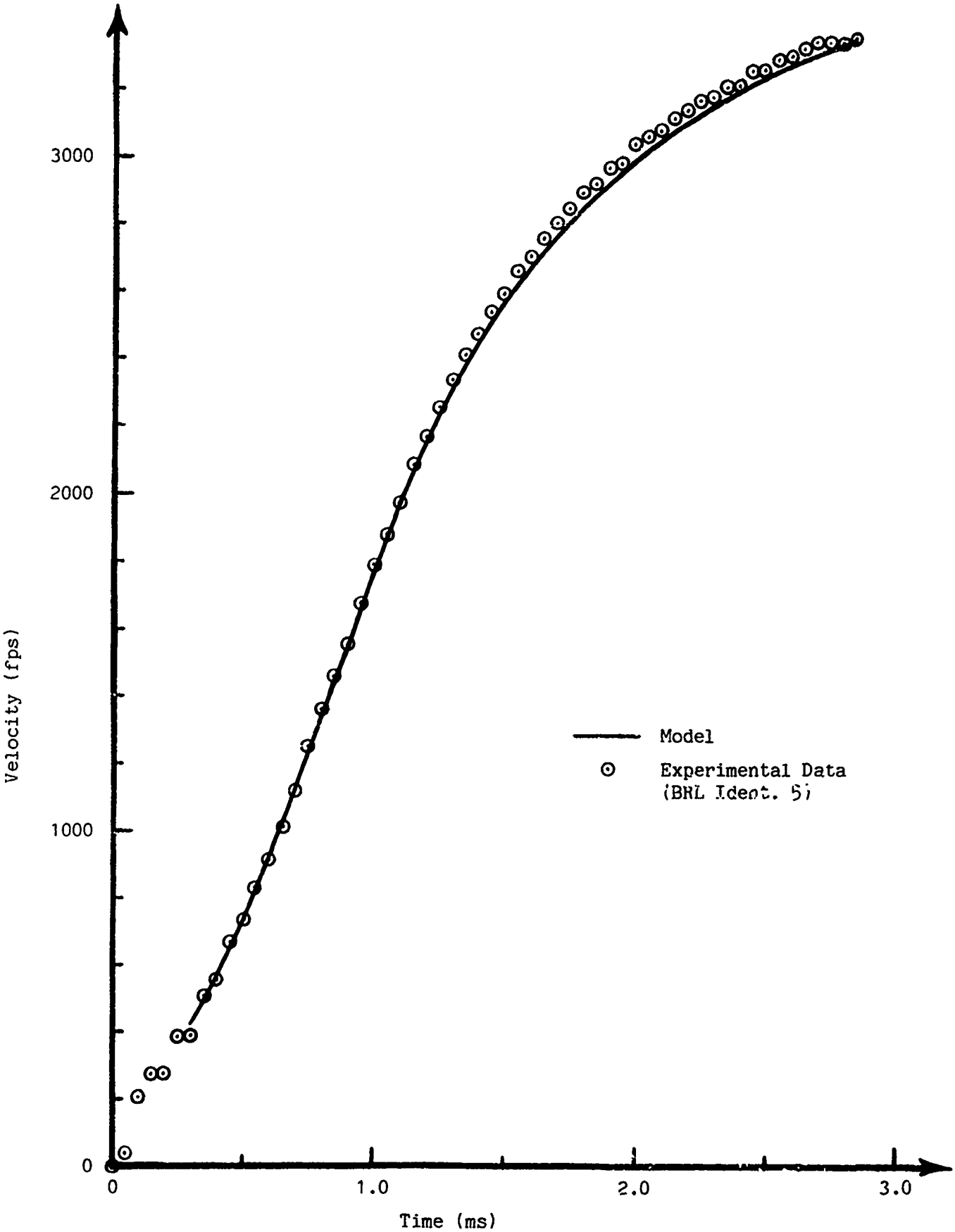

Figure 16 - Velocity-Time Correlation (Short Round with Balloting)

Balloting motion as predicted by the model for this projectile is illustrated in Figure 17; which shows the time-dependent variation of the maximum radial displacement at the bourrelet. In addition, the positions of secondary peaks obtained from the experimental radar doppler "waterfall" plot for this round are also indicated in this figure. Equating these peaks with maximum balloting (as indicated by bourrelet/bore impacts) yields good agreement with the dominant response frequency predicted by the model, especially in the mid-section of the in-bore motion. Variation of the experimentally derived frequency in the neighborhood of shot-exit, and the poorer correlation in this region, may reflect the effects of bore wear near the muzzle, as well as dynamic erosion of the rotating band (neither of which are accounted for within the model). Model output further indicated that the magnitude and frequency of balloting is dominated by projectile yaw and pitch. This is illustrated in Figure 18, wherein yaw versus pitch is presented relative to the inertial reference frame, S'.

4.4 General Observations

In view of the excellent overall correlation with the experimental data, several general observations regarding model predictions for balloting rounds are not only pertinent, but have important ramifications regarding gun tube motion and shot accuracy. In particular, model output for balloting rounds reveals high frequency content and large magnitudes in projectile/bore interfacial loading, as well as transverse linear and angular velocities.

Referring to Figure 17, three distinct frequencies are discernible in the balloting motion of the projectile as predicted by the model. The dominant frequency of approximately 5,000 Hz is attributable to pitch and yaw motion. Superimposed on this dominant motion is a higher frequency of approximately 50,000 Hz, discernible primarily at the extremes of pitching motion and attributable to radial displacement of the projectile c.g. Finally, a much lower frequency of approximately 700 Hz is discernible as amplitude modulation of the dominant mode and is attributable to interior ballistics pressure and projectile/bore interfacial friction loads.

Further insight into the origin of the higher frequencies of balloting motion may be gained by examination of the expressions for the transverse loads and moments generated at the rotating band/bore interface as given

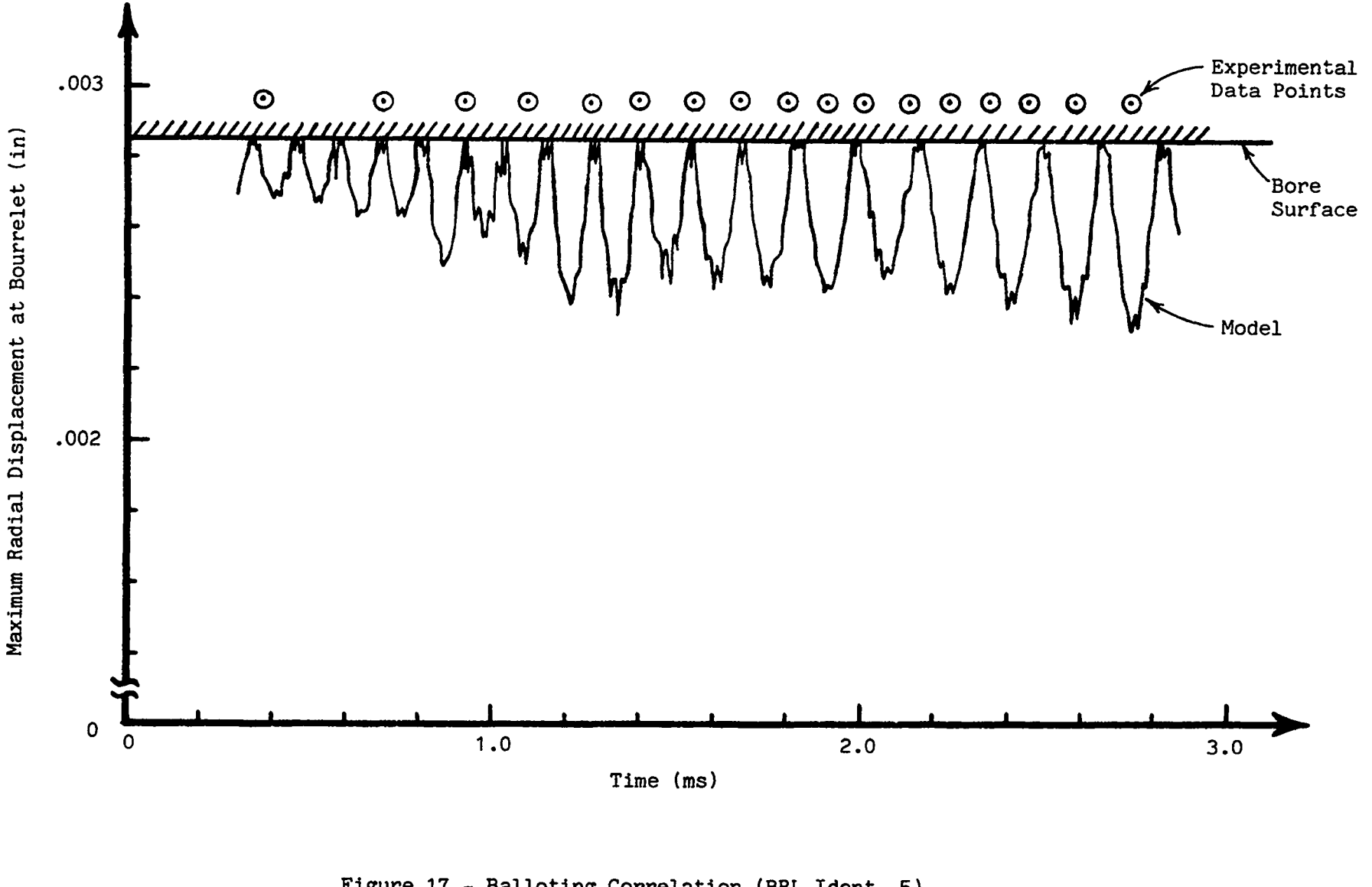

Figure 17 - Balloting Correlation (BRL Ident. 5)

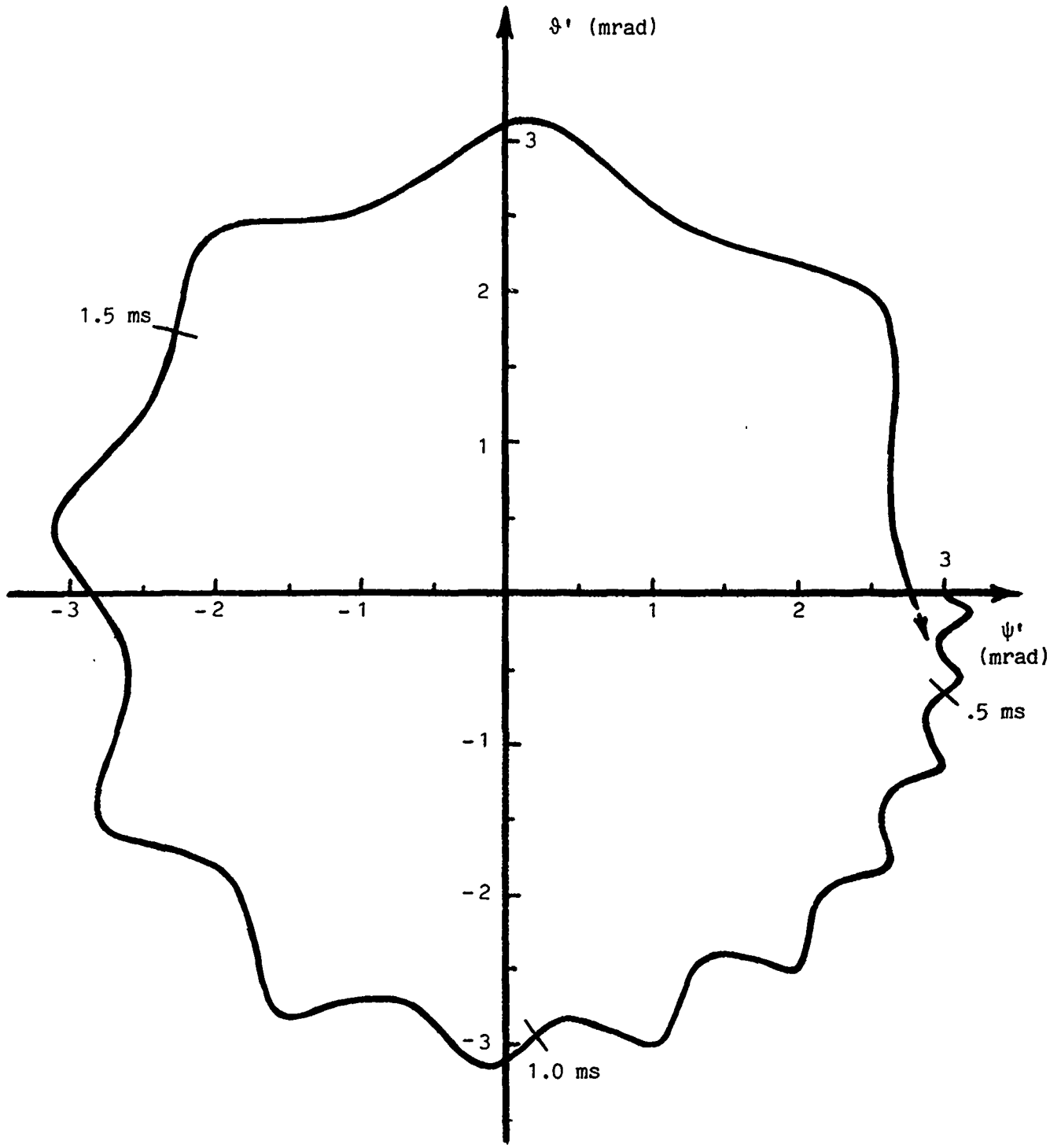

Figure 18 - Model Prediction of Projectile Yaw versus Pitch

respectively by equations (58) and (61). Referring to equation (58), an effective radial-load stiffness, k_r, may be defined as

$$k_r = \pi\, r_b\, k' \quad . \tag{86}$$

Similarily, referring to equation (61), an effective "foundation" moment stiffness, C_M, may be defined as

$$C_M = \frac{\pi\, r_b\, h^2\, k'}{12} \quad . \tag{87}$$

Based on these stiffnesses, theoretical natural frequencies for radial (linear) motion, defined as k_r/m_p, and pitch and/or yaw (angular) motion defined as C_M/I_{zz} and/or C_M/I_{yy}, were calculated for the short round. These theoretical frequencies, namely 45,000 Hz (linear) and 4,500 Hz (angular), correlate well with the frequencies observed in Figure 17. (Actual model output frequencies are expected to be somewhat higher since the projectile is not in a free-vibration mode, its response being modified by bore impacts.)

It should be noted that model output for the balloting projectile indicated that the rotating-band/bore interfacial loads and moments (associated with the stiffnesses given in equations (86) and (87)) have maximum values of the order of 10,000 lb and 1,000 in-lb, respectively. In contrast, output for non-balloting projectiles indicated interfacial loads three orders of magnitude lower. Similarily, balloting projectiles evidence much higher transverse linearand angular velocities; approaching orders of 10 in/sec and 10 rad/sec, respectively. Such relatively high transverse velocities would be expected to adversely affect projectile "jump" at shot-exit, and hence, overall shot accuracy.

In summary, model output indicates that balloting projectiles experience high frequency, large magnitude interfacial loads determined primarily by the physical characteristics of the rotating band. These loads, which cannot be accounted for in point-mass projectile approximations, have the potential to affect gun tube motion via "feedback."

Since the formulation presented in Section 2 also addressed application to smoothbore gun tubes, two additional program runs were performed beyond the correlation study in an attempt to contrast rifled and smoothbore firings. One

run was performed for a rifled gun tube without twist; a second run was performed for a smoothbore gun tube by modifying the computer program to reflect the additional degree of freedom, φ_o, in the equations of motion, as well as the required changes in the impact equations (as noted in Section 2). For the purpose of comparison, both runs utilized the same inputs and initial conditions as were used for the short balloting round.

With the exception of projectile spin, comparison of the output from these two runs showed identical results for the motion of the projectile. The smoothbore case exhibited a monotonically increasing function for $\dot{\varphi}_o$, with a maximum value of 5 mrad/sec at shot-exit; whereas, the straight rifling, of course, constrained the projectile to zero spin. Comparison of either of these runs with the run with rifling twist showed that balloting induced by the same initial state of malengraving is markedly attenuated by gyroscopic stabilization. This is seen in Figure 19, which presents a comparison of the instantaneous pitch angle for spinning and non-spinning (or smoothbore) projectiles. As is seen in Figure 19, there is a marked increase in pitch magnitude and velocity, as well as in the number of bourrelet/bore impacts, for the non-spinning projectile. Output further indicated that the magnitude of the impulse transmitted at bourrelet/bore impact was also significantly greater for the non-spinning projectile.

Finally, a comparison of the affect of balloting on the longitudinal motion of a projectile is illustrated in Figure 20, wherein model output are presented for a perfectly aligned, spinning projectile (without bore impacts or balloting motion), as well as spinning and non-spinning, balloting projectiles. As is seen from this figure, balloting adversely affects muzzle velocity; propellant energy which would otherwise contribute to projectile muzzle velocity in a non-balloting situation is expended in sustaining balloting motion.

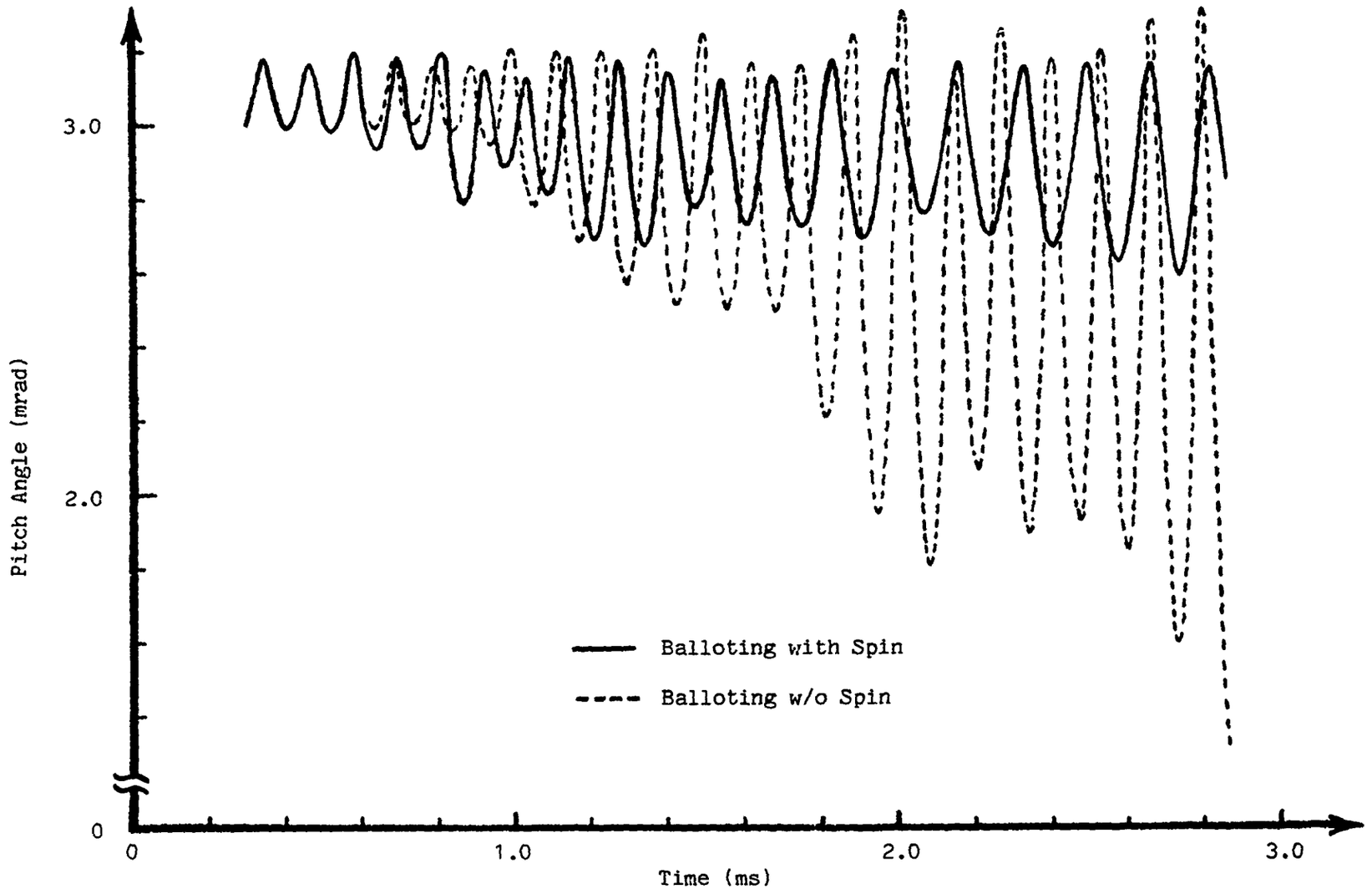

Figure 19 - Pitching Motion Comparison

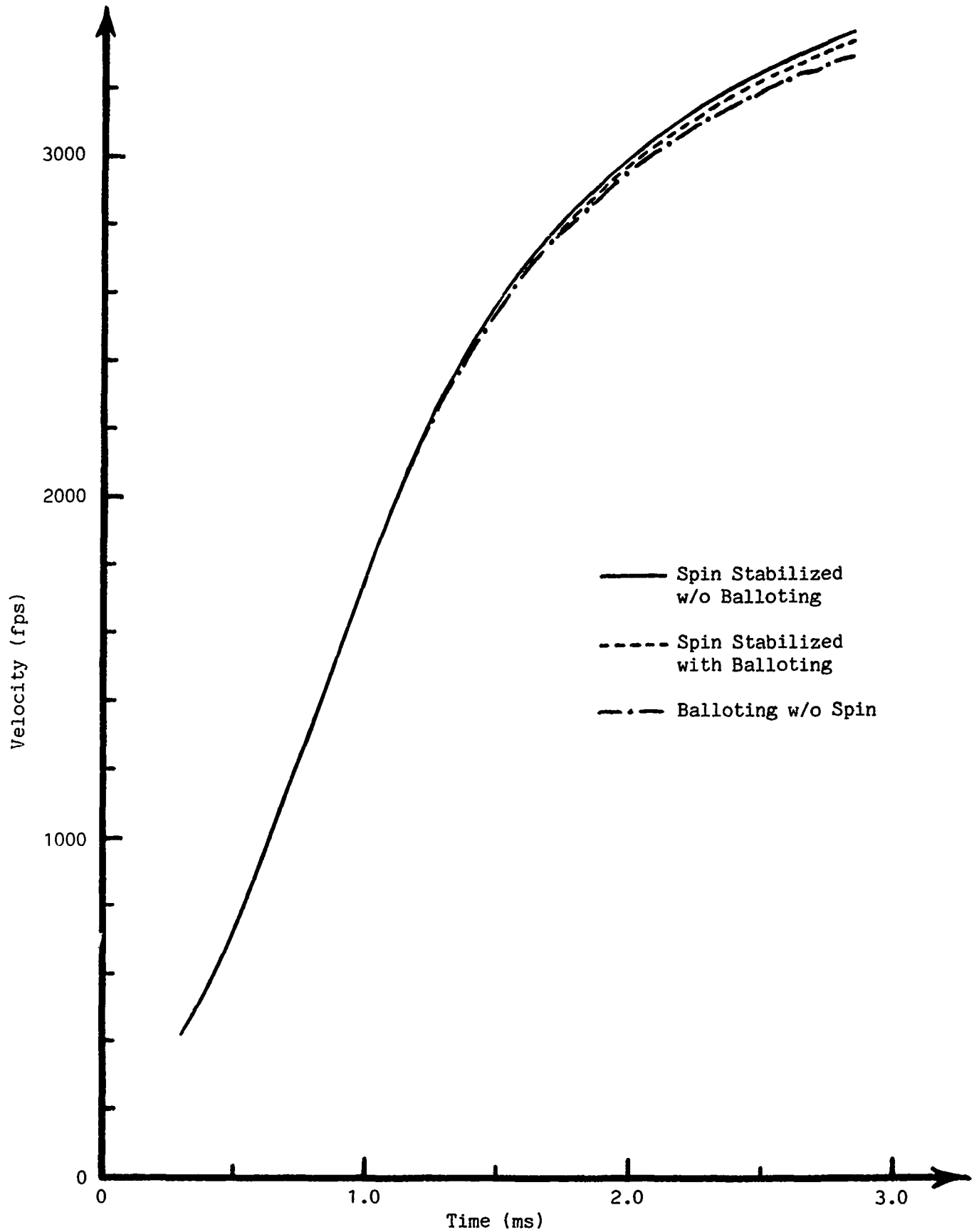

Figure 20 - Velocity Comparison

SECTION 5

INCORPORATION OF MODEL WITHIN DYNACODE-G

Incorporation of the model herein developed within DYNACODE-G requires consideration of the nature of the equations of motion and interfacial loads and moments presented in Section 2, as well as the general observations noted in Section 4.

With respect to the formulation presented in Section 2, it is noted that projectile/gun-tube motions are fundamentally coupled through kinematic, as well as loading constraints. Kinematic coupling is manifested by terms entering the projectile equations of motion which relate the instantaneous orientation and motion of the reference frame S_o to the reference frame S'. Specifically, the Euler angles $(\psi_o,\vartheta_o,\varphi_o)$ and the coordinates (x',y',z') are identified with local gun-tube slopes, torque and displacements defined in DYNACODE-G. Referring to the projectile, these quantities (and their time derivatives) may be viewed as "driving" forces entering the projectile equations of motion. Physically, these "driving" forces are transmitted to the projectile via loadings acting at the rotating-band/bore and bourrelet/bore interfaces. Alternately, referring to the gun tube, projectile "feedback" to gun tube motion is manifested through equal and opposite reaction loads and moments which must be applied to the gun tube within DYNACODE-G; thereby "driving" the gun tube. Hence, introduction of the model within DYNACODE-G offers the ability to assess the mutual effects of projectile/gun-tube interaction previously unattainable via a point-mass projectile description.

Two additional points are noteworthy. As was seen in Section 4, a balloting projectile in an otherwise perfectly symmetric and "ideal" gun system has the potential to induce gun tube motion. Conversely, gun tube motion has the potential to induce balloting in an otherwise perfectly aligned and symmetric projectile.

To fully account for the above noted coupling, incorporation of the model within DYNACODE-G requires simultaneous integration of the differential equations presented in Section 2 with the equation set characterizing the generalized, time-dependent amplitudes of the gun system normal modes defined in DYNACODE-G. In addition, the present sub-routine which computes the instantaneous loading on the gun tube due to motion of a point-mass projectile is to be replaced by a routine incorporating the loads and moments developed in

Section 2.3.

As was discussed in Section 4, projectile balloting is dominated by frequencies approaching the natural frequencies of the rotating band in angular and radial modes respectively. Because of the relatively high values of these frequencies, integration of the projectile equations of motion for the parameters ψ, ϑ, y_{cg}, and z_{cg} required an integration step-size of 2.5 μsec to achieve a stable, convergent solution. In contrast, previous applications of DYNACODE-G have demonstrated stable, convergent solutions with an integration step-size of 25 μsec (accommodating gun system natural frequencies to 1,000 Hz). In the interest of computational economy, it is conceivable to integrate projectile parameters at the smaller step-size, while utilizing interpolation for gun system parameters integrated at the coarser step. However, it is highly likely that the presence of projectile balloting will induce excitation of higher order gun system modes in greater proportion than have appeared in previous applications. Should this be the case, convergence and stability of the solution for gun system parameters would require a smaller integration step-size. In light of these comments, it is recommended that initial runs of the combined code be performed with the smallest, constant time-step leading to stable, convergent solutions for both projectile and gun system parameters.

Exercising appropriate caution in integrating the combined code will greatly enhance our understanding of the mutual interaction between projectile and gun system. For example, program output will be valuable in quantifying projectile "jump" conditions at shot-exit (relative to either the gun tube or an inertial reference). In addition, the combined code could be used on a deterministic basis to quantify shot-to-shot variations resulting, for example, from variations in interior ballistics pressure, projectile asymmetries or the degree of projectile malengraving.

SECTION 6

CONCLUSIONS AND RECOMMENDATIONS

A rigorous formulation of the general, six degree-of-freedom motion of a projectile of finite geometry and inertia traveling in a flexible (rifled or smoothbore) gun tube has been developed. The formulation accommodates projectile spin, mass eccentricity, projectile/bore interfacial friction, elastic/plastic deformation of the projectile rotating band, and balloting--including bourrelet impact and rebound with the bore. The formulation has been developed in a form compatible with DYNACODE-G, such that incorporation within the latter provides the ability to assess the mutual effects of projectile/gun-tube interaction during in-bore motion. The formulation has been compared with other projectile in-bore motion formulations and descriptions appearing in recent literature, and has been found to be the most general developed to date. In addition, the formulation has been correlated with experimental in-bore radar doppler data provided by the U.S. Army Ballistic Research Laboratory for firings of a specially designed 37mm weapon, and has been found to provide excellent agreement for rounds which exhibit balloting, as well as rounds which exhibit little or no evidence of balloting.

Referring to the model output presented in Section 4 for the particular projectile designs therein considered, several observations regarding balloting are in order. First, the onset of balloting is dictated by the state of the projectile when fully engraved (i.e., the total amount of malengraving) and/or the presence of mass eccentricity. Second, balloting motion subsequent to engraving, and in the absence of gun tube motion feedback, is dictated primarily by the design of the rotating band and, in particular, the relative magnitude of the "foundation" moment stiffness. Third, several distinct frequencies are discernible in the balloting motion of the projectiles considered: a dominant frequency of approximately 5,000 Hz, dictated primarily by the response frequency of the rotating band in the "foundation" moment mode; a higher, superimposed frequency of approximately 50,000 Hz, discernible at the extrema of displacement in the bourrelet-plane and dictated primarily by the radial response frequency of the rotating band; finally, a much lower frequency of approximately 700 Hz, discernible as amplitude modulation of the dominant frequency and primarily attributable to the interior ballistics pressure and projectile/bore interfacial friction loads. Fourth, gyroscopic stabilization

(due to spin) has a marked affect on the attenuation of balloting, affecting the loads transmitted through the rotating band and bourrelet, as well as the linear and angular velocities of the projectile throughout its in-bore travel and, in particular, at shot exit. Fifth, overall balloting motion as predicted by the model is of more consistent nature in terms of frequency content than is indicated in the experimental data provided, especially as the projectile approaches the neighborhood of the muzzle.

A final observation, although speculative at this point, is nevertheless noteworthy. Gun tube motion predictions based on theoretical simulations generally contain considerably lower frequency content than do corresponding experimental data (e.g., accelerometer data). Perhaps this disparity, which to date has been viewed by many investigators as an experimental anomaly, arises as a consequence of mutual projectile/gun-tube interaction. The finding noted in Section 4, namely, that relatively high projectile/bore interfacial loads are found to exist in a balloting situation, lends credence to this speculation.

In view of the demonstrated merits of the model herein developed and its potentially broad range of applicability, as well as its potential for resolving the theoretical/experimental disparity noted above, it is strongly recommended that this study be extended for the purpose of incorporating the model within DYNACODE-G, as discussed in Section 5. In addition, in view of the importance of accurately defining the state of the projectile immediately following engraving, as well as defining variations in projectile/bore clearances due to wear and erosion of both the bore and rotating band (particularly in the latter stages of in-bore travel), it is recommended that additional effort be expended in modeling these processes (via introduction of stochastic techniques, where applicable).

ACKNOWLEDGEMENTS

S&D Dynamics, Inc. and, in particular, the authors, wish to express their appreciation to the U.S. Army Research Office and, in particular, to Dr. Frederick W. Schmiedeshoff of the Engineering Sciences Division for supporting this effort.

In addition, we also wish to express our appreciation to Mr. James O. Pilcher II and Dr. James N. Walbert of the Mechanics and Structures Branch,

Interior Ballistics Laboratory, U.S. Army Ballistic Research Laboratory, for their valuable technical input and support during the course of this effort, and to Miss Susan A. Coates of the Mechanics and Struccures Branch for performing the analog-to-digital conversion of the 37mm in-bore radar doppler data needed to establish an experimental basis for model validation.

REFERENCES

1. "Dynamic Analysis of the 75mm ADMAG Gun System," S&D Dynamic, Inc., BRL Contract Report ARBRL-CR-00495, December 1982. (AD# ADA 123867)

2. Soifer, M.T. and Becker, R.S., "Gun Dynamics Simulation Model of the 75mm ADMAG Gun System," Proceedings of the Third US Army Symposium on Gun Dynamics, Volume I, pp. I-48 thru I-71, 11-14 May 1982.

3. Chu, S.H., "New Approach for Analysis of Transverse Projectile-Tube Interactions," Proceedings of the Third US Army Symposium on Gun Dynamics, Volume II, pp. III-106 thru III-125, 11-14 May 1982.

4. "Dynamics of a Projectile in a Concentric Flexible Tube," BLM Applied Mechanics Associates, BRL Contract Report ARBRL-CR-00501, February 1983. (AD# ADA 125481)

5. Wu, J.J., "On Dynamic Forces in Gun Tube Motion Analysis," Proceedings of the Third US Army Symposium on Gun Dynamics, Volume II, pp. III-85 thru III-97, 11-14 May 1982.

6. Simkins, T.E., "Transverse Response of Gun Tubes to Curvature-Induced Load Functions," Proceedings of the Second US Army Symposium on Gun Dynamics, pp. I-67 thru I-77, 19-22 September 1978.

7. "Muzzle Motions of the M68 105-MM Tank Gun," Southwest Research Institute, BRL Contract Report ARBRL-CR-00418, March 1980. (AD# ADB046954)

8. Haug, E.J., Chun, Y.W., Song, J.O., and Hou, J.W., "Dynamic and Design Sensitivity Analysis of a Gun Tube with Ballistic Excitation," Materials Division, College of Engineering, University of Iowa, Final Report under Contract No. DAAA22-78-C-0202 to the Benet Weapons Laboratory, Watervliet, N.Y., July 1979.

9. Walbert, J.N., "Techniques for the Analysis of Radar Doppler from Projectiles in the In-Bore and Early Free-Flight Regions," U.S. Army Ballistic Research Laboratory (awaiting publication).

10. Walbert, J.N., "Analysis of the In-Bore Motion of Several Types of Projectiles," U.S. Army Ballistic Research Laboratory (awaiting publication).

11. Hill, R., The Mathematical Theory of Plasticity, Chap. V, Sect. 2, Oxford University Press, London, 1971.

12. Soifer, M.T., "Interior Ballistics Model with Traveling Propellant Charge," Final Report prepared for Frankford Arsenal under Task Order 72-593 to Battelle Memorial Institute, Columbus Laboratories, October 1973.

13. Courant, R. and Friedrichs, K.O., Supersonic Flow and Shock Waves, Chap. III, Sect. 67-69, Interscience Publishers, Inc., New York, 1963.

APPENDIX A

INSTANTANEOUS ANGULAR ORIENTATION

APPENDIX A

The instantaneous angular orientation and velocity of the intermediate reference frame, S_o, with coordinates (x_o, y_o, z_o) and unit triad $(\hat{i}_o, \hat{j}_o, \hat{k}_o)$, are obtained relative to the inertial reference frame, S', with coordinates (x', y', z') and unit triad $(\hat{i}', \hat{j}', \hat{k}')$, in terms of the Euler angles $(\psi_o, \vartheta_o, \varphi_o)$ defined in Figure A-1.

Beginning with S_o initially coincident with S', the instantaneous angular orientation of S_o relative to S' at any later time is (referring to Figure A-1) obtained by subjecting S_o to the following consecutive rotations:

(i) ψ_o *about z', bringing x' to its final elevation, ξ, and y' to its intermediate orientation, η;*

(ii) ϑ_o *about η, bringing ξ to its final azimuth, x_o, and z' to its final azimuth, ζ;*

(iii) φ_o *about x_o, bringing η to its final orientation, y_o, and ζ to its final elevation, z_o.*

The direction cosines, ℓ^o_{ij}, defining the transformation between S_o and S' at any instant are obtained by noting the relation between the unit triads depicted in Figure A-1 subsequent to each consecutive rotation, as follows:

(i) following the rotation ψ_o, there results

$$\hat{i}' = \cos\psi_o\,\hat{i}_\xi - \sin\psi_o\,\hat{i}_\eta \tag{A-1}$$

$$\hat{j}' = \sin\psi_o\,\hat{i}_\xi + \cos\psi_o\,\hat{i}_\eta \tag{A-2}$$

(ii) following the rotation ϑ_o, there results

$$\hat{i}_\xi = \cos\vartheta_o\,\hat{i}_o + \sin\vartheta_o\,\hat{i}_\zeta \tag{A-3}$$

$$\hat{k}' = -\sin\vartheta_o\,\hat{i}_o + \cos\vartheta_o\,\hat{i}_\zeta \tag{A-4}$$

(iii) following the rotation φ_o, there results

$$\hat{i}_\eta = \cos\varphi_o\,\hat{j}_o - \sin\varphi_o\,\hat{k}_o \tag{A-5}$$

$$\hat{i}_\zeta = \sin\varphi_o\,\hat{j}_o + \cos\varphi_o\,\hat{k}_o \quad . \tag{A-6}$$

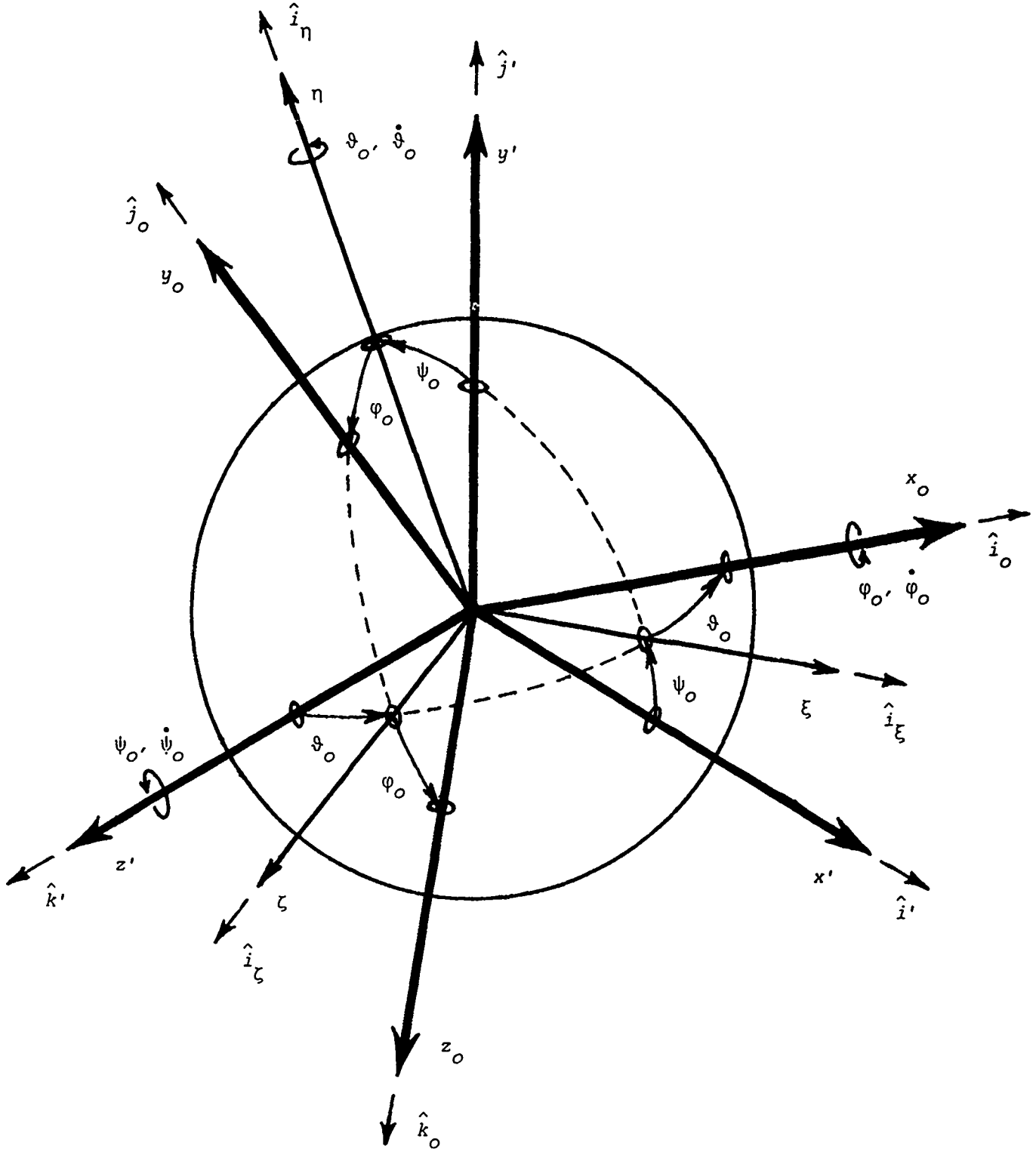

Figure A-1. *Definition of Euler Angles*

Eliminating the unit triad $(\hat{i}_\xi, \hat{i}_\eta, \hat{i}_\zeta)$ *associated with the intermediate coordinates* (ξ, η, ζ) *there results the transformation as given in equation (5), with the direction cosines as defined in equation (6).*

Referring again to Figure A-1, it is seen that the angular velocity of S_o *relative to S', namely* $\bar{\omega}_o$, *is given as*

$$\bar{\omega}_o = \dot{\psi}_o \hat{k}' + \dot{\vartheta}_o \hat{i}_\eta + \dot{\varphi}_o \hat{i}_o \ . \qquad \text{(A-7)}$$

Once again using the above transformations between unit triads, there results $\bar{\omega}_o$ *in the form as given in equation (12); with components as defined in equation (13).*

NOMENCLATURE

English Symbols

A	- projected areas of rotating band and bourrelet
$\bar{a}$	- total translational acceleration of projectile c.g. relative to S'
$\bar{a}_{cg}$	- acceleration of projectile c.g. relative to S_o
$\bar{a}_o$	- acceleration of origin of S_o relative to S'
a_p	- projectile acceleration along gun tube axis
a_{x_o}, a_{y_o}, a_{z_o}	- components of $\bar{a}_o$ relative to S_o
C_M	- effective "foundation" moment stiffness
c	- propellant charge
$d\bar{F}_c$	- resultant incremental contact load acting on a differential element of the rotating band
$dF^c_{x_o}$, $dF^c_{y_o}$, $dF^c_{z_o}$	- components of $d\bar{F}_c$ relative to S_o
E	- Young's modulus for rotating band material
e	- coefficient of restitution
$\bar{F}$	- resultant applied load acting on projectile
$\hat{\bar{F}}$	- impulsive load at bourrelet/bore interface
$\bar{F}_a$	- "ram" air pressure load
$\bar{F}_b$	- projectile base pressure load
$\bar{F}_p$	- resultant pressure load
$\bar{F}_w$	- projectile weight load
F_{x_o}, F_{y_o}, F_{z_o}	- components of $\bar{F}$ relative to S_o
$F^c_{x_o}$, $F^c_{y_o}$, $F^c_{z_o}$	- components of rotating-band/bore interfacial loads relative to S_o
$F^p_{x_o}$, $F^p_{y_o}$, $F^p_{z_o}$	- components of $\bar{F}_p$ relative to S_o
$F^w_{x_o}$, $F^w_{y_o}$, $F^w_{z_o}$	- components of $\bar{F}_w$ relative to S_o
g	- gravitational acceleration

$\bar{H}$ - total angular momentum of projectile

h - rotating band width

$I_{xx}, I_{yy}, \ldots, I_{yz}$ - elements of projectile inertia tensor relative to S

$(\hat{i},\hat{j},\hat{k})$ - unit triad associated with S

$(\hat{i}',\hat{j}',\hat{k}')$ - unit triad associated with S'

$(\hat{i}_o,\hat{j}_o,\hat{k}_o)$ - unit triad associated with S_o

$\hat{i}_r$ - radial unit-vector at bore surface

k - elastic "spring" stiffness per unit surface area of rotating band

k' - "spring" stiffness per unit circumferential length of rotating band

k_r - effective radial-load stiffness of rotating band

$\bar{\ell}_a$ - moment arm from projectile c.g. to "ram" air load

ℓ_b - perpendicular distance from projectile c.g. to rear face of rotating band

$\bar{\ell}_b$ - moment arm from projectile c.g. to base pressure load

$\bar{\ell}_M$ - moment arm of incremental contact load at rotating-band/bore interface

ℓ_1 - perpendicular distance from projectile c.g. to forward face of bourrelet

ℓ_{ij} (i,j=1,2,3) - direction cosines between S and S_o

ℓ^o_{ij} (i,j=1,2,3) - direction cosines between S_o and S'

$\bar{M}$ - resultant applied moment acting about projectile c.g.

M_p - ratio of projectile speed to ambient air sound speed

$\bar{M}_p$ - moment due to pressure loads

M_x, M_y, M_z - components of $\bar{M}$ relative to S

M^c_x, M^c_y, M^c_z - components relative to S of moment due to rotating-band/bore interfacial contact

M^p_x, M^p_y, M^p_z - components of $\bar{M}_p$ relative to S

$M^c_{x_o}, M^c_{y_o}, M^c_{z_o}$ - components relative to S_o of moment due to rotating-band/bore interfacial contact

m_p - projectile mass

p_a - "ram" air pressure

p_b - projectile base pressure

p_c - chamber pressure

p_o - ambient air pressure

$\bar{R}$ - radial load per unit surface area of rotating band

$\hat{R}$ - radially directed impulsive load acting at bourrelet/bore interface

$\bar{r}$ - position vector of projectile c.g. relative to origin of S'

r_b - bore radius

$\bar{r}_{cg}$ - position vector of projectile c.g. relative to origin of S_o

r_i - inner radius of rotating band

r_o - outer radius of rotating band

$\bar{r}_o$ - position vector of origin of S_o relative to origin of S'

$\bar{r}_1$ - position vector from projectile c.g. to point of bourrelet/bore impact

S - projectile body-fixed reference frame

S' - inertial reference frame

S_o - intermediate (gun tube) reference frame

s - distance along gun tube axis

$\bar{T}$ - rifling torque-load per unit surface area of rotating band

t - time

t_w - rifling twist

$\bar{v}$ - total translational velocity of projectile c.g. relative to S'

$\bar{v}'_c$ - velocity of bourrelet impact-point relative to the bore

$\bar{v}_{cg}$ - velocity of projectile c.g. relative to S_o

$\bar{v}'_{cg}$ - velocity of projectile c.g. relative to the gun tube

$\bar{v}_o$ - velocity of origin of S_o relative to S'

v_p - projectile velocity along gun tube axis

v_{x_o}, v_{y_o}, v_{z_o} - components of $\bar{v}_o$ relative to S_o

(x,y,z) - orthogonal coordinates of S

(x',y',z') - orthogonal coordinates of S'

(x_o,y_o,z_o) - orthogonal coordinates of S_o

y_{cg}, z_{cg} - projectile c.g. displacements in $\hat{j}_o$-$\hat{k}_o$ plane

Greek Symbols

α - angular orientation of friction load at rotating-band/bore interface

γ - specific heat ratio of air

$\bar{\delta}$ - transverse displacement of any point in a plane perpendicular to projectile geometric axis

δ_{max} - maximum radial displacement

δ_o - initial radial compression of rotating band

δ_r - radial component of $\bar{\delta}$

ε - projectile c.g. offset from geometric axis

ϑ' - projectile yaw relative to S'

μ - friction coefficient at rotating-band/bore interface

μ_1 - friction coefficient at bourrelet/bore interface

ν - Poisson's ratio

ξ - distance from projectile c.g. to any plane perpendicular to geometric axis of projectile

$\hat{\bar{\tau}}$ - impulsive torque generated at rotating-band/bore interface due to bourrelet/bore impact

φ - Euler angle of S relative to S_o; also, angle between projection of y_o-axis and line from gun tube centerline to point in plane of interest

φ_{max} - angular orientation of maximum radial displacement

φ_o - Euler angle of S_o relative to S'; also, projectile spin angle

φ_1 - angular orientation of bourrelet/bore impact-point

$(\psi, \vartheta, \varphi)$ - Euler angles of S relative to S_o

ψ' - projectile pitch relative to S'

$(\psi_o, \vartheta_o, \varphi_o)$ - Euler angles of S_o relative to S'

$\bar{\omega}$ - total angular velocity of projectile relative to S'

$\dot{\bar{\omega}}$ - total angular acceleration of projectile relative to S'

$\bar{\omega}_{cg}$ - angular velocity of projectile relative to S_o

$\dot{\bar{\omega}}_{cg}$ - angular acceleration of projectile relative to S_o

$\bar{\omega}_o$ - angular velocity of S_o relative to S'

$\dot{\bar{\omega}}_o$ - angular acceleration of S_o relative to S'

$\omega_x, \omega_y, \omega_z$ - components of $\bar{\omega}$ relative to S

$\dot{\omega}_x, \dot{\omega}_y, \dot{\omega}_z$ - components of $\dot{\bar{\omega}}$ relative to S

$\omega_{x_{cg}}, \omega_{y_{cg}}, \omega_{z_{cg}}$ - components of $\bar{\omega}_{cg}$ relative to S

$\dot{\omega}_{x_{cg}}, \dot{\omega}_{y_{cg}}, \dot{\omega}_{z_{cg}}$ - components of $\dot{\bar{\omega}}_{cg}$ relative to S

$\omega_{x_o}, \omega_{y_o}, \omega_{z_o}$ - components of $\bar{\omega}_o$ relative to S_o

$\dot{\omega}_{x_o}, \dot{\omega}_{y_o}, \dot{\omega}_{z_o}$ - components of $\dot{\bar{\omega}}_o$ relative to S_o

Additional Notation

$\hat{(\ )}$ - unit vector; also, impulsive load

$\bar{(\ )}$ - vector quantity

$\partial(\ )$ - partial derivative

$d(\ )$ - total (convective) derivative

$\dot{(\ )}$ - derivative with respect to time

$\Delta(\ )$ - "jump" (sudden increment) in parameter due to bourrelet/bore impact

$(\ )^+$ - value of parameter immediately subsequent to impact

$(\ )^-$ - value of parameter just prior to impact

DISTRIBUTION LIST

No. of Copies	Organization
12	Administrator Defense Technical Info Center ATTN: DTIC-DDA Cameron Station Alexandria, VA 22314
1	Commander USA Materiel Command ATTN: AMCDRA-ST 5001 Eisenhower Avenue Alexandria, VA 22333
1	Commander USA BMD Advanced Technology Center ATTN: BMDATC-M, P. Boyd P.O. Box 1500 Huntsville, AL 35807
1	Commander USA Materiel Command ATTN: AMCLDC 5001 Eisenhower Avenue Alexandria, VA 22333
5	Commander USA AMCCOM, ARDC ATTN: SMCAR-TDC, D. Gyorog SMCAR-LC SMCAR-SE SMCAR-SA SMCAR-AC Dover, NJ 07801
1	Commander USA AMCCOM, ARDC ATTN: SMCAR-TSS Dover, NJ 07801
1	Commandant US Army Infantry School ATTN: ATSH-CD-CSO-OR Fort Benning, GA 31905
1	Commander US Army Development & Employment Agency ATTN: MODE-TED-SAB Fort Lewis, WA 98433
5	Commander USA AMCCOM, ARDC ATTN: SMCAR-LCU, E. Barrieres SMCAR-LCU, R. Davitt SMCAR-LCU-M, D. Robertson SMCAR-LCU-M, M. Weinstock SMCAR-LCA, C. Larson Dover, NJ 07801
3	Commander USA AMCCOM, ARDC ATTN: SMCAR-LCA, B. Knutelski SMCAR-LCR-R, E.H. Moore III SMCAR-LCS-D, K. Rubin Dover, NJ 07801
7	Commander USA AMCCOM, ARDC ATTN: SMCAR-SCM SMCAR-SCS, B. Brodman SMCAR-SCS, T. Hung SMCAR-SCA, W. Gadomski SMCAR-SCA, E. Malatesta SMCAR-SCA-T, P. Benzkofer SMCAR-SCA-T, F. Dahdouh Dover, NJ 07801
3	Commander USA AMCCOM, ARDC ATTN: SMCAR-LCR, W. Williver SMCAR-LCA, S. Bernstein SMCAR-LCN, G. Demitrack Dover, NJ 07801
4	Commander USA AMCCOM, ARDC ATTN: SMCAR-LCA, S. Yim SMCAR-LCA, L. Rosendorf SMCAR-LCA, S.H. Chu SMCAR-LCW, R. Wrenn Dover, NJ 07801
1	AFWL/SUL Kirtland AFB, NM 87117
1	HQDA DAMA-ART-M Washington, DC 20310

DISTRIBUTION LIST

No. of Copies	Organization
2	Director USA AMCCOM, ARDC Benet Weapons Laboratory ATTN: SMCAR-LCB-RA, T. Simkins SMCAR-D, J. Zweig Watervliet, NY 12189
1	Director USA AMCCOM, ARDC Benet Weapons Laboratory ATTN: SMCAR-LCB-TL Watervliet, NY 12189
1	Commander USA AMCCOM ATTN: Product Assurance Dir. SMCAR-QAR-RIB D. Imhof Dover, NJ 07801
1	Commander USA AMCCOM, ARDC ATTN: SMCAR-TSE, L. Goldsmith Dover, NJ 07801
1	Commander USA ARRCOM ATTN: AMSMC-TSE-SW, R. Radkiewicz Rock Island, IL 61299
1	Commander USA ARRCOM ATTN: AMSMC-LEP-L Rock Island, IL 61299
1	Commander USA Aviation Research and Development Command ATTN: AMSAV-E 4300 Goodfellow Blvd. St. Louis, MO 63120
1	Director USA Air Mobility Research and Development Laboratory Ames Research Center Moffett Field, CA 94035
1	Commander USA Communications Research and Development Command ATTN: AMSEL-ATDD Fort Monmouth, NJ 07703
1	Commander USA Electronics Research and Development Command Technical Support Activity ATTN: AMDSD-L Fort Monmouth, NJ 07703
3	Commander USA Harry Diamond Laboratories ATTN: DELHD-I-TR, H.D. Curchak DELHD-I-TR, H. Davis DELHD-S-QE-ES, B. Banner 2800 Powder Mill Road Adelphi, MD 20783
1	Commander USA Harry Diamond Laboratories ATTN: DELHD-TA-L 2800 Powder Mill Road Adelphi, MD 20783
1	Commander USA Missile Command ATTN: AMSMI-R Redstone Arsenal, AL 35898
1	Commander USA Missile Command ATTN: AMSMI-YDL Redstone Arsenal, AL 35898
1	Commander USA Tank Automotive Command ATTN: AMSTE-TSL Warren, MI 48090

DISTRIBUTION LIST

No. of Copies	Organization
2	Commander USA Jefferson Proving Ground ATTN: STEJP-TD-O, A. Tilley STEJP-TD-E, J. Toomey Madison, IN 47251
1	Director USA TRADOC Systems Analysis Activity ATTN: ATAA-SL WSMR, NM 88002
2	Commander USA Yuma Proving Ground ATTN: STEYP-MTW, R. Torp G. Stullenbarger Yuma, AZ 85365
1	Commander USA Research Office ATTN: E. Saibel P.O. Box 12211 Research Triangle Park NC 27709
2	Commander USA Research Office P.O. Box 12211 ATTN: Engineering Division Metallurgy & Materials Division Research Triangle Park NC 27709
2	Project Manager Nuclear Munitions ATTN: AMCPM-NUC Dover, NJ 07801
2	Project Manager Tank Main Armament Systems ATTN: AMCPM-TMA Dover, NJ 07801
2	Project Manager ATTN: AMCPM-ADG, Sergeant York Dover, NJ 07801
3	Project Manager Cannon Artillery Weapons Systems ATTN: AMCPM-CAWS US Army AMCCOM Dover, NJ 07801
1	Product Manager for 30mm Ammo ATTN: AMCPM-AAH-30mm Dover, NJ 07801
2	Product Manager M110E2 Weapon System, DARCOM ATTN: AMCPM -M110E2 Rock Island, IL 61299
2	Commander USA Materials and Mechanics Research Center ATTN: J. Mescall Tech. Library Watertown, MA 02172
1	Commander Naval Sea Systems Command (SEA-035.3) ATTN: L. Pasiuk Washington, DC 20360
1	Commander Naval Explosive Ordnance Disposal Facility ATTN: Lib Div Indian Head, MD 20640
1	Superintendent Naval Postgraduate School ATTN: Dir of Lib Monterey, CA 93940
1	Commander Naval Surface Weapons Center ATTN: G-13, W.D. Ralph Dahlgren, VA 22448

DISTRIBUTION LIST

No. of Copies	Organization
5	Commander Naval Surface Weapons Center ATTN: Code G-33, T.N. Tschirn Code N-43, J.J. Yagla L. Anderson G. Soo Hoo Code TX, W.G. Soper Dahlgren, VA 22448
2	Commander Naval Weapons Center ATTN: Code 3835, R. Sewell Code 3431, Tech Lib China Lake, CA 93555
2	Commander US Naval Weapons Center ATTN: Code 608, R. Derr Code 4505, C. Thelen China Lake, CA 93555
2	Commander Naval Ordnance Station ATTN: Code 5034, C. Irish, T.C. Smith Indian Head, MD 20640
2	AFATL Gun and Rocket Division Gun Test Branch AD3246 TEST W/TETFG ATTN: D. Davis DLDL Eglin AFB, FL 32542
1	Southwest Research Institute ATTN: P. Cox 8500 Culebra Road San Antonio, TX 78228
1	AFELM, The Rand Corporation ATTN: Library-D 1700 Main Street Santa Monica, CA 90406
1	S&D Dynamics, Inc. 755 New York Ave. Huntington, NY 11743

No. of Copies	Organization
3	Commanding General US Army Tank Automotive Cmd ATTN: AMCPM -GCM-SW, L. Wolcott R. Walsh AMCPM -M1E1, J. Raffiani Warren, MI 48090
	Aberdeen Proving Ground Dir, USAMSAA ATTN: AMXSY-D AMXSY-MP, H. Cohen Cdr, USATECOM ATTN: AMSTE-TO-F
	Dir, USAMTD ATTN: D. Dykstra J. Fasig S. Walton
	Cdr, CRDC, AMCCOM ATTN: SMCCR-RSP-A SMCCR-MU SMCCR-SPS-IL